A wave finite element approach for the analysis of periodic structures with cyclic symmetry in dynamic substructuring

Jean-Mathieu Mencik

A wave finite element approach for the analysis of periodic structures with cyclic symmetry in dynamic substructuring

Jean-Mathieu Mencik

INSA Centre Val de Loire, Université d'Orléans, Université de Tours, Laboratoire de Mécanique Gabriel Lamé, 3 Rue de la Chocolaterie, F-41034 Blois, France

Abstract

A numerical approach is proposed to compute the dynamic response of periodic structures with cyclic symmetry, and assemblies made up of these periodic structures. The wave finite element (WFE) method is used to describe the wave modes which occur around the circumferential direction of these periodic structures. Emphasis is placed on assessing the dynamic flexibility modes of a periodic structure by considering unit forces which are successively applied to the boundary degrees of freedom. It is shown that the matrices of dynamic flexibility modes can be quickly computed. This yields an efficient dynamic substructuring technique to analyze the dynamic behavior of assemblies made up of several periodic structures. Numerical experiments are carried out which concern the analysis of a single periodic structure as well as assemblies made up of two and three structures.

Key words: wave finite element method, periodic structures, cyclic symmetry, dynamic flexibility modes, dynamic substructuring.

1. Introduction

A numerical approach is proposed to compute the dynamic response of periodic structures with cyclic symmetry. Such systems are frequently encountered in the aeronautic industry in the design of turbines. Predicting their dynamic behavior by means of accurate and efficient numerical tools has become a key challenge which is motivated by the need of considering systems of increasing complexity — i.e., systems which involve finite element (FE) models with many degrees of freedom (DOFs). To address this issue, the FE method [1] and the theory of cyclic symmetry [2] can be used. However, both of these approaches suffer from strong issues. These mainly concern the numerical cost involved when assembling and inverting large-sized sparse matrices in an FE model, and, concerning the theory of cyclic symmetry, the use of an assumption consisting of neglecting the coupling between the harmonic modes (nodal diameters) of two connected periodic structures [3]. As a result, the CPU times involved in the FE method are likely to be excessive, while the accuracy of the theory of cyclic symmetry cannot be guaranteed when coupled systems are dealt with. The present paper aims at proposing an alternative approach to circumvent these drawbacks.

A new numerical approach is proposed which involves considering the wave finite element (WFE) method. In this framework, the so-called wave modes of a periodic structure with cyclic symmetry are computed. These are to be understood as the waves which propagate/travel around the circumferential direction of the structure. The wave modes are further used to express the dynamic flexibility modes of the structure, which is done by analyzing its dynamic response when unit forces are applied to the boundary DOFs. The interesting and original feature of the proposed approach is that the matrices of dynamic flexibility modes can be quickly computed, leading the way to an efficient dynamic substructuring technique to analyze assemblies made up of several periodic structures.

Email address: jean-mathieu.mencik@insa-cvl.fr (Jean-Mathieu Mencik)

Basically, the WFE method can be viewed as a transfer matrix approach to describe the wave propagation along one-dimensional periodic structures, i.e., structures composed of identical substructures which are connected to each other along a straight or circumferential direction. So far, the WFE method has been applied to different kinds of homogeneous and heterogeneous structures [4–9], elasto-acoustic systems [10, 11], poroelastic media [12], and so on. The WFE method works by considering the FE model of a substructure — i.e., a periodicity pattern which can have arbitrary 2D or 3D shape — which can be obtained using a commercial FE software. Hence, the dynamic stiffness matrix (DSM) of the substructure can be expressed (from the known mass, damping and stiffness matrices) which is further condensed on the interface DOFs, that is, those on the coupling interfaces with the previous and subsequent substructures. By considering the condensed DSM, the transfer matrix of the substructure can be expressed. It links the displacement and force vectors on one interface of the substructure (say, the right boundary) to those on the second one (left boundary). The wave modes of a periodic structure are finally obtained by computing the eigenvalues and eigenvectors of the transfer matrix of the substructure. These are referred to as the wave parameters (wave numbers) and the wave mode shapes, respectively.

Also, the WFE method has been applied to compute the harmonic forced response of periodic structures [13–17]. In this framework, finite-length periodic structures — i.e., structures with a finite number of substructures — are dealt with, whose ends can be subject to different kinds of boundary or coupling conditions. In this case, assumption is made that the DOFs which do not belong to the end boundaries of the periodic structures are free from excitation sources. The WFE strategy consists in expressing the displacement and force vectors of a periodic structure, at the substructure interfaces, in terms of wave mode shapes. This yields small-sized wave-based matrix equations which can be solved efficiently. The analysis of assemblies made up of periodic structures which are coupled together (on their end boundaries), or which are coupled to elastic junctions, can be undertaken in the same way and requires the coupling conditions to be expressed in wave-based forms. The interesting feature of the WFE method is that it is faster than the FE method, while keeping the same level of accuracy.

In addition, it should be emphasized that the WFE method has been applied to the analysis of two-dimensional periodic structures like bi-periodic plates built from a 2D array of identical substructures [18]. This approach has been mostly applied to identify Bloch waves in 2D periodic structures, and analyze the related band gap effects, i.e., frequency regions on which Bloch waves do not propagate. The counterpart of this approach, however, is that it is restricted to the analysis of the 2D wave propagation in infinite periodic structures. The analysis of bounded structures, e.g., with a surrounding boundary on which boundary conditions are considered, is an extremely tough issue which has never been carried out so far from the author's point of view. The scientific challenge mostly relies on the modeling of the reflection and transmission phenomena of Bloch waves, which are multi-directive, on the boundary of the periodic structures.

The underlying question behind the WFE method, for one-dimensional periodic structures, may be stated as to how to widen its range of application so that it can be applied to real engineering problems. In [19], it has been shown that the WFE method is capable of handling periodic structures made up of arbitrary shaped substructures whose FE models can contain many DOFs (e.g., more than $10,000$). One main limitation of the WFE method, however, is that the excitation sources are considered at the structure ends, which especially means that the substructures are supposed to be free from excitations. The present work aims at tackling this problem within the specific scope of periodic structures with cyclic symmetry, e.g., with an inner circumferential boundary subject to a distributed excitation. This leads the way to the analysis of coupled problems involving several periodic structures with cyclic symmetry which are connected together around their boundaries. In this sense, a dynamic substructuring technique can be proposed in the framework of which several periodic structures are modeled in terms of dynamic flexibility modes. The analysis of assemblies made up of several periodic structures follows from a domain decomposition procedure by enforcing displacement continuity conditions at coupling DOFs.

The scientific novelties of the present work can be summarized as follows:

- Modeling of periodic structures with cyclic symmetry whose inner circumferential boundary is subject

to a distributed excitation.

- Numerical approach for quickly computing the matrices of dynamic flexibility modes of periodic structures, and modeling assemblies made up of several periodic structures which are connected together across their inner circumferential boundaries.

The rest of the paper is organized as follows. In Section 2.1, the FE model of a substructure which is used in the WFE method is presented. The WFE strategy for computing the wave modes of periodic structures with cyclic symmetry is presented in Section 2.2. Also, the WFE strategy for computing the forced response of periodic structures with cyclic symmetry is detailed in Section 2.3. In Section 2.4, the derivation of the matrices of dynamic flexibility modes is proposed. The analysis of assemblies made up of several periodic structures is proposed in Section 2.5. Finally, numerical experiments are brought in Section 3. These concern the study of one single periodic structure (Section 3.1), and assemblies made up of two and three periodic structures (Sections 3.2 and 3.3). The relevance of the WFE approach is analyzed through comparisons with the FE method and the theory of cyclic symmetry.

2. Theory

2.1. Problem description

Consider a periodic structure with cyclic symmetry, made up of identical substructures as shown in Figure 1. In the frequency domain, the FE model of a substructure can be expressed by the following dynamic equilibrium matrix equation:

$$\begin{bmatrix} \mathbf{D}_{\Gamma\Gamma} & \mathbf{D}_{\Gamma\mathtt{I}} \\ \mathbf{D}_{\Gamma\mathtt{I}}^T & \mathbf{D}_{\mathtt{I}\mathtt{I}} \end{bmatrix} \begin{bmatrix} \mathbf{q}_\Gamma \\ \mathbf{q}_\mathtt{I} \end{bmatrix} = \begin{bmatrix} \mathbf{F}_\Gamma \\ \mathbf{F}_\mathtt{I} \end{bmatrix}, \tag{1}$$

where $\mathbf{q}$ and $\mathbf{F}$ refer to the displacement vector and force vector, respectively; subscripts Γ and $\mathtt{I}$ refer, respectively, to the interface DOFs — i.e., the coupling interfaces with the other substructures — and the internal DOFs — i.e., the remaining DOFs (see Figure 1). Also, the matrix on the left-hand side of Eq. (1) is the DSM of the substructure — namely $\mathbf{D}$ — which is symmetric and expressed by $\mathbf{D} = -\omega^2\mathbf{M} + (1 + \mathtt{i}\eta)\mathbf{K}$ where $\mathbf{M}$ is the mass matrix, $\mathbf{K}$ is the stiffness matrix, ω is the angular frequency, η is the loss factor and $\mathtt{i}$ is the unit imaginary number.

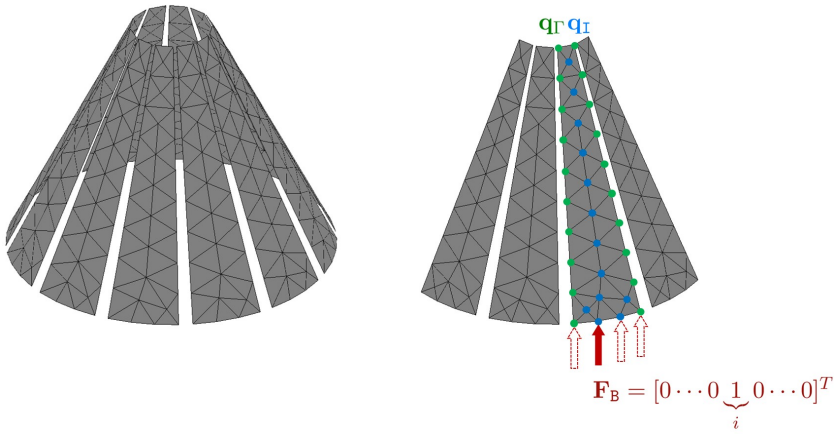

Figure 1: Periodic structure with one substructure excited by a unit force on a boundary DOF i (in this case, the boundary refers to the bottom edge).

Regarding Figure 1, the internal DOFs of the substructures are assumed to be free from excitations, i.e., $\mathbf{F}_\mathtt{I} = \mathbf{0}$, except one substructure which is excited by a unit force on a boundary DOF i. The boundary DOFs of the substructures are to be understood as defining a certain region over which the whole periodic structure can

be subject to excitation sources and coupled with a second periodic structure. For the particular case displayed in figure 1, the boundary DOFs of the substructures refer to the bottom edge. Here, the vector of boundary forces for the excited substructure is expressed as follows:

$$\mathbf{F}_{\mathtt{B}} = [0 \cdots 0 \underbrace{1}_{i} 0 \cdots 0]^T. \tag{2}$$

Notice that the boundary DOFs belong to the set encompassing both the interface and internal DOFs. Hence, the force vector in Eq. (1) should be partitioned accordingly. This yields:

$$\begin{bmatrix} \mathbf{D}_{\Gamma\Gamma} & \mathbf{D}_{\Gamma\mathtt{I}} \\ \mathbf{D}_{\Gamma\mathtt{I}}^T & \mathbf{D}_{\mathtt{II}} \end{bmatrix} \begin{bmatrix} \mathbf{q}_\Gamma \\ \mathbf{q}_{\mathtt{I}} \end{bmatrix} = \begin{bmatrix} \mathbf{F}_\Gamma + \mathcal{L}_{\Gamma\mathtt{B}}\mathbf{F}_{\mathtt{B}} \\ \mathcal{L}_{\mathtt{IB}}\mathbf{F}_{\mathtt{B}} \end{bmatrix}, \tag{3}$$

where $\mathcal{L}_{\Gamma\mathtt{B}}$ and $\mathcal{L}_{\mathtt{IB}}$ are Boolean localization matrices, and $\mathbf{F}_\Gamma$ is the vector of coupling forces between the excited substructure and the non-excited connected substructures.

Within the WFE framework, one needs to consider the condensed DSM of a substructure which is obtained by condensing the internal DOFs on the interface DOFs. Notice that the direct computation of the condensed DSM is usually cumbersome for substructures with many internal DOFs. To solve this issue, the Craig Bampton (CB) method can be used [20]. The procedure has been proposed in [14] and is detailed hereafter for the sake of clarity.

The idea behind the CB method is to express the displacement vector $\mathbf{q}_{\mathtt{I}}$ in terms of static modes and a reduced number of fixed interface modes, as follows:

$$\mathbf{q}_{\mathtt{I}} \approx \mathbf{X}_{\mathtt{st}}\mathbf{q}_\Gamma + \widetilde{\mathbf{X}}_{\mathtt{el}}\widetilde{\boldsymbol{\alpha}}, \tag{4}$$

where $\mathbf{X}_{\mathtt{st}}$ is the matrix of static modes expressed by $\mathbf{X}_{\mathtt{st}} = -\mathbf{K}_{\mathtt{II}}^{-1}\mathbf{K}_{\mathtt{IB}}$, and $\widetilde{\mathbf{X}}_{\mathtt{el}} = [\widetilde{\boldsymbol{\xi}}_1 \cdots \widetilde{\boldsymbol{\xi}}_{m_{\mathtt{el}}}]$ is the reduced matrix of fixed interface modes $\widetilde{\boldsymbol{\xi}}_j$, with $m_{\mathtt{el}}$ the number of fixed interface modes retained which is supposed to be small compared to the number of internal DOFs of the substructure; also, $\widetilde{\boldsymbol{\alpha}}$ is a $m_{\mathtt{el}} \times 1$ vector of generalized coordinates. The fixed interface modes $\widetilde{\boldsymbol{\xi}}_j$ are the solutions of the equation $\mathbf{K}_{\mathtt{II}}\widetilde{\boldsymbol{\xi}}_j = \lambda_j \mathbf{M}_{\mathtt{II}}\widetilde{\boldsymbol{\xi}}_j$, which is a generalized eigenproblem involving the stiffness and mass matrices $(\mathbf{K}_{\mathtt{II}}, \mathbf{M}_{\mathtt{II}})$ associated to the internal DOFs of the substructure. Here, the eigenvalues λ_j have the meaning of the square of the eigenpulsations of the substructure with fixed interfaces. The strategy to select the fixed interface modes consists in retaining those for which the eigenpulsations are under a certain threshold, e.g., twice the maximum pulsation within the frequency band analyzed.

To sum up, the displacement vector of the substructure can be approximated as follows:

$$\begin{bmatrix} \mathbf{q}_\Gamma \\ \mathbf{q}_{\mathtt{I}} \end{bmatrix} \approx \mathbf{T} \begin{bmatrix} \mathbf{q}_\Gamma \\ \widetilde{\boldsymbol{\alpha}} \end{bmatrix} \qquad \text{where} \quad \mathbf{T} = \begin{bmatrix} \mathbf{I} & \mathbf{0} \\ \mathbf{X}_{\mathtt{st}} & \widetilde{\mathbf{X}}_{\mathtt{el}} \end{bmatrix}. \tag{5}$$

Following the Galerkin projection method, Eq. (3) leads to

$$\mathbf{T}^T \begin{bmatrix} \mathbf{D}_{\Gamma\Gamma} & \mathbf{D}_{\Gamma\mathtt{I}} \\ \mathbf{D}_{\Gamma\mathtt{I}}^T & \mathbf{D}_{\mathtt{II}} \end{bmatrix} \mathbf{T} \begin{bmatrix} \mathbf{q}_\Gamma \\ \widetilde{\boldsymbol{\alpha}} \end{bmatrix} = \mathbf{T}^T \begin{bmatrix} \mathbf{F}_\Gamma + \mathcal{L}_{\Gamma\mathtt{B}}\mathbf{F}_{\mathtt{B}} \\ \mathcal{L}_{\mathtt{IB}}\mathbf{F}_{\mathtt{B}} \end{bmatrix}, \tag{6}$$

which yields

$$\begin{bmatrix} \mathbf{D}_{\mathtt{st-st}} & \widetilde{\mathbf{D}}_{\mathtt{st-el}} \\ \widetilde{\mathbf{D}}_{\mathtt{st-el}}^T & \widetilde{\mathbf{D}}_{\mathtt{el-el}} \end{bmatrix} \begin{bmatrix} \mathbf{q}_\Gamma \\ \widetilde{\boldsymbol{\alpha}} \end{bmatrix} = \begin{bmatrix} \mathbf{F}_\Gamma + \left(\mathcal{L}_{\Gamma\mathtt{B}} + \mathbf{X}_{\mathtt{st}}^T\mathcal{L}_{\mathtt{IB}}\right)\mathbf{F}_{\mathtt{B}} \\ \widetilde{\mathbf{X}}_{\mathtt{el}}^T\mathcal{L}_{\mathtt{IB}}\mathbf{F}_{\mathtt{B}} \end{bmatrix}. \tag{7}$$

The block terms occurring in the matrix on the left hand side of Eq. (7) result from the matrix multiplication $\mathbf{T}^T\mathbf{D}\mathbf{T}$ in Eq. (6). The condensed DSM of the substructure is obtained as follows. From Eq. (7), the vector of generalized coordinates $\widetilde{\boldsymbol{\alpha}}$ is expressed by

$$\widetilde{\boldsymbol{\alpha}} = \widetilde{\mathbf{D}}_{\mathtt{el-el}}^{-1}(\widetilde{\mathbf{X}}_{\mathtt{el}}^T\mathcal{L}_{\mathtt{IB}}\mathbf{F}_{\mathtt{B}} - \widetilde{\mathbf{D}}_{\mathtt{st-el}}^T\mathbf{q}_\Gamma). \tag{8}$$

As a result, Eq. (7) yields

$$\mathbf{D}^*\mathbf{q}_\Gamma = \mathbf{F}_\Gamma + \left(\mathcal{L}_{\Gamma\mathtt{B}} + (\mathbf{X}_{\mathtt{st}}^T - \widetilde{\mathbf{D}}_{\mathtt{st-el}}\widetilde{\mathbf{D}}_{\mathtt{el-el}}^{-1}\widetilde{\mathbf{X}}_{\mathtt{el}}^T)\mathcal{L}_{\mathtt{IB}}\right)\mathbf{F}_{\mathtt{B}}, \tag{9}$$

where $\mathbf{D}^*$ is the condensed DSM of the substructure, expressed by

$$\mathbf{D}^* = \mathbf{D}_{\mathtt{st-st}} - \widetilde{\mathbf{D}}_{\mathtt{st-el}}\widetilde{\mathbf{D}}_{\mathtt{el-el}}^{-1}\widetilde{\mathbf{D}}_{\mathtt{st-el}}^T. \tag{10}$$

Eq. (9) represents the dynamic equilibrium equation of a substructure whose boundary DOFs are excited. For a non-excited substructure, since $\mathbf{F}_{\mathtt{B}} = \mathbf{0}$, one simply has:

$$\mathbf{D}^*\mathbf{q}_\Gamma = \mathbf{F}_\Gamma. \tag{11}$$

Eq. (11) is the starting point of the WFE method which will be developed in the next subsection.

2.2. WFE method

Consider a periodic structure made up of N identical substructures as shown in Figure 1, with a rotational periodicity of $2\Delta\theta$, and denote as (k) $(k = 1, 2, \ldots, N)$ the coupling interfaces between the substructures. Also, assume that the substructures are free from external excitations other than coupling forces with the other substructures. It should be emphasized that N substructures are considered which are arranged in ascending order around a closed circle. Hence, the last substructure (say, substructure N) connects to the first substructure (substructure 1) on the coupling interface (1).

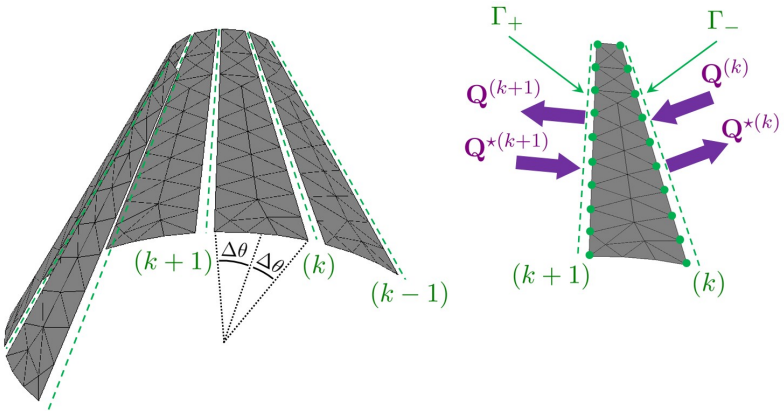

Figure 2: FE mesh of a periodic structure with a rotational periodicity of $2\Delta\theta$ (left), and FE mesh of a substructure (right).

For the sake of clarity, a substructure which is enclosed between two interfaces (k) and $(k+1)$ is shown in Figure 2. Denote as Γ_- and Γ_+ the sides of the substructure which match the interfaces (k) and $(k+1)$, respectively. Also, assume that Γ_- and Γ_+ are meshed in the same way with the same number n of DOFs, and let us rewrite Eq. (11) as follows:

$$\begin{bmatrix} \mathbf{D}^*_{\Gamma_-\Gamma_-} & \mathbf{D}^*_{\Gamma_-\Gamma_+} \\ \mathbf{D}^*_{\Gamma_+\Gamma_-} & \mathbf{D}^*_{\Gamma_+\Gamma_+} \end{bmatrix} \begin{bmatrix} \mathbf{q}^{(k)}_{\Gamma_-} \\ \mathbf{q}^{(k+1)}_{\Gamma_+} \end{bmatrix} = \begin{bmatrix} \mathbf{F}^{(k)}_{\Gamma_-} \\ \mathbf{F}^{(k+1)}_{\Gamma_+} \end{bmatrix}. \tag{12}$$

Eq. (12) is usually expressed in cartesian coordinates. However, within the framework of rotational periodicity, it has to be expressed in cylindrical coordinates as follows. Assume, without loss of generality, that each node of the FE mesh of the substructure is modeled with 3 translational DOFs, and define the axis $\theta = 0$ as the mid-plane (y, z) of the substructure. Then, consider two 3×3 transformation matrices $\mathcal{T}_-$ and $\mathcal{T}_+$ to link the unit

vectors in cylindrical coordinates — say, $(\vec{e}_r, \vec{e}_\theta, \vec{e}_z)$ — to the unit vectors in cartesian coordinates $(\vec{e}_x, \vec{e}_y, \vec{e}_z)$ when $\theta = -\Delta\theta$ and $\theta = \Delta\theta$, respectively. Hence,

$$\begin{bmatrix} \vec{e}_r \\ \vec{e}_\theta \\ \vec{e}_z \end{bmatrix} = \mathcal{T}_- \begin{bmatrix} \vec{e}_x \\ \vec{e}_y \\ \vec{e}_z \end{bmatrix} \quad \text{when } \theta = -\Delta\theta \qquad , \qquad \begin{bmatrix} \vec{e}_r \\ \vec{e}_\theta \\ \vec{e}_z \end{bmatrix} = \mathcal{T}_+ \begin{bmatrix} \vec{e}_x \\ \vec{e}_y \\ \vec{e}_z \end{bmatrix} \quad \text{when } \theta = \Delta\theta. \tag{13}$$

Expressions of the displacement and force vectors, on Γ_- and Γ_+, in cylindrical coordinates follow as:

$$\widehat{\mathbf{q}}^{(k)}_{\Gamma_-} = (\mathbf{I}_{n/3} \otimes \mathcal{T}_-)\mathbf{q}^{(k)}_{\Gamma_-} \quad , \quad \widehat{\mathbf{F}}^{(k)}_{\Gamma_-} = (\mathbf{I}_{n/3} \otimes \mathcal{T}_-)\mathbf{F}^{(k)}_{\Gamma_-}, \tag{14}$$

and

$$\widehat{\mathbf{q}}^{(k+1)}_{\Gamma_+} = (\mathbf{I}_{n/3} \otimes \mathcal{T}_+)\mathbf{q}^{(k+1)}_{\Gamma_+} \quad , \quad \widehat{\mathbf{F}}^{(k+1)}_{\Gamma_+} = (\mathbf{I}_{n/3} \otimes \mathcal{T}_+)\mathbf{F}^{(k+1)}_{\Gamma_+}, \tag{15}$$

where symbol $\widehat{\bullet}$ means that vectors/matrices are expressed in cylindrical coordinates. Also, $\otimes$ is the Kronecker product and $n/3$ is the number of nodes on each interface Γ_- or Γ_+. Notice that the transformation matrices $\mathcal{T}_-$ and $\mathcal{T}_+$ are orthogonal, i.e., $\mathcal{T}_-^{-1} = \mathcal{T}_-^T$ and $\mathcal{T}_+^{-1} = \mathcal{T}_+^T$. As a result, Eq. (12) can be expressed in cylindrical coordinates as follows:

$$\begin{bmatrix} \widehat{\mathbf{D}}^*_{\Gamma_-\Gamma_-} & \widehat{\mathbf{D}}^*_{\Gamma_-\Gamma_+} \\ \widehat{\mathbf{D}}^*_{\Gamma_+\Gamma_-} & \widehat{\mathbf{D}}^*_{\Gamma_+\Gamma_+} \end{bmatrix} \begin{bmatrix} \widehat{\mathbf{q}}^{(k)}_{\Gamma_-} \\ \widehat{\mathbf{q}}^{(k+1)}_{\Gamma_+} \end{bmatrix} = \begin{bmatrix} \widehat{\mathbf{F}}^{(k)}_{\Gamma_-} \\ \widehat{\mathbf{F}}^{(k+1)}_{\Gamma_+} \end{bmatrix}, \tag{16}$$

where

$$\widehat{\mathbf{D}}^*_{\Gamma_-\Gamma_-} = (\mathbf{I}_{n/3} \otimes \mathcal{T}_-)\mathbf{D}^*_{\Gamma_-\Gamma_-}(\mathbf{I}_{n/3} \otimes \mathcal{T}_-^T) \quad , \quad \widehat{\mathbf{D}}^*_{\Gamma_+\Gamma_+} = (\mathbf{I}_{n/3} \otimes \mathcal{T}_+)\mathbf{D}^*_{\Gamma_+\Gamma_+}(\mathbf{I}_{n/3} \otimes \mathcal{T}_+^T), \tag{17}$$

$$\widehat{\mathbf{D}}^*_{\Gamma_-\Gamma_+} = (\mathbf{I}_{n/3} \otimes \mathcal{T}_-)\mathbf{D}^*_{\Gamma_-\Gamma_+}(\mathbf{I}_{n/3} \otimes \mathcal{T}_+^T) \quad , \quad \widehat{\mathbf{D}}^*_{\Gamma_+\Gamma_-} = (\mathbf{I}_{n/3} \otimes \mathcal{T}_+)\mathbf{D}^*_{\Gamma_+\Gamma_-}(\mathbf{I}_{n/3} \otimes \mathcal{T}_-^T). \tag{18}$$

In condensed form, Eqs. (15), (14), (17) and (18) give:

$$\begin{bmatrix} \widehat{\mathbf{q}}^{(k)}_{\Gamma_-} \\ \widehat{\mathbf{q}}^{(k+1)}_{\Gamma_+} \end{bmatrix} = \mathcal{H} \begin{bmatrix} \mathbf{q}^{(k)}_{\Gamma_-} \\ \mathbf{q}^{(k+1)}_{\Gamma_+} \end{bmatrix} \quad , \quad \begin{bmatrix} \widehat{\mathbf{F}}^{(k)}_{\Gamma_-} \\ \widehat{\mathbf{F}}^{(k+1)}_{\Gamma_+} \end{bmatrix} = \mathcal{H} \begin{bmatrix} \mathbf{F}^{(k)}_{\Gamma_-} \\ \mathbf{F}^{(k+1)}_{\Gamma_+} \end{bmatrix} \quad , \quad \widehat{\mathbf{D}}^* = \mathcal{H}\mathbf{D}^*\mathcal{H}^T, \tag{19}$$

where

$$\mathcal{H} = \begin{bmatrix} (\mathbf{I}_{n/3} \otimes \mathcal{T}_-) & \mathbf{0} \\ \mathbf{0} & (\mathbf{I}_{n/3} \otimes \mathcal{T}_+) \end{bmatrix}. \tag{20}$$

From Eq. (16), a transfer matrix relation can be expressed which links the displacement and force vectors at the interface $(k+1)$ to those at the previous interface (k) [21]:

$$\begin{bmatrix} \widehat{\mathbf{q}}^{(k+1)}_{\Gamma_+} \\ \widehat{\mathbf{F}}^{(k+1)}_{\Gamma_+} \end{bmatrix} = \widehat{\mathbf{S}} \begin{bmatrix} \widehat{\mathbf{q}}^{(k)}_{\Gamma_-} \\ -\widehat{\mathbf{F}}^{(k)}_{\Gamma_-} \end{bmatrix}. \tag{21}$$

Here, $\widehat{\mathbf{S}}$ denotes the transfer matrix (size $2n \times 2n$), expressed by

$$\widehat{\mathbf{S}} = \begin{bmatrix} -\widehat{\mathbf{D}}^{*-1}_{\Gamma_-\Gamma_+}\widehat{\mathbf{D}}^*_{\Gamma_-\Gamma_-} & -\widehat{\mathbf{D}}^{*-1}_{\Gamma_-\Gamma_+} \\ \widehat{\mathbf{D}}^*_{\Gamma_+\Gamma_-} - \widehat{\mathbf{D}}^*_{\Gamma_+\Gamma_+}\widehat{\mathbf{D}}^{*-1}_{\Gamma_-\Gamma_+}\widehat{\mathbf{D}}^*_{\Gamma_-\Gamma_-} & -\widehat{\mathbf{D}}^*_{\Gamma_+\Gamma_+}\widehat{\mathbf{D}}^{*-1}_{\Gamma_-\Gamma_+} \end{bmatrix}. \tag{22}$$

It can be proven that the matrix $\widehat{\mathbf{S}}$ is symplectic [21, 22], which means that $\widehat{\mathbf{S}}^T\mathbf{J}\widehat{\mathbf{S}} = \mathbf{J}$, where

$$\mathbf{J} = \begin{bmatrix} \mathbf{0} & \mathbf{I}_n \\ -\mathbf{I}_n & \mathbf{0} \end{bmatrix}. \tag{23}$$

Consider now the coupling conditions between two consecutive substructures, e.g., on an interface (k). This gives

$$\begin{bmatrix} \widehat{\mathbf{q}}_{\Gamma_-}^{(k)} \\ -\widehat{\mathbf{F}}_{\Gamma_-}^{(k)} \end{bmatrix} = \begin{bmatrix} \widehat{\mathbf{q}}_{\Gamma_+}^{(k)} \\ \widehat{\mathbf{F}}_{\Gamma_+}^{(k)} \end{bmatrix}. \tag{24}$$

Eq. (24) means that the displacements are continuous across the coupling interface, while the coupling forces satisfy the action-reaction law. Hence, by considering Eqs. (21) and (24), this yields the following transfer matrix relation between two consecutive substructures:

$$\begin{bmatrix} \widehat{\mathbf{q}}_{\Gamma_+}^{(k+1)} \\ \widehat{\mathbf{F}}_{\Gamma_+}^{(k+1)} \end{bmatrix} = \widehat{\mathbf{S}} \begin{bmatrix} \widehat{\mathbf{q}}_{\Gamma_+}^{(k)} \\ \widehat{\mathbf{F}}_{\Gamma_+}^{(k)} \end{bmatrix}. \tag{25}$$

Hence, the transfer matrix $\widehat{\mathbf{S}}$ links the displacement and force vectors between two consecutive substructures, on their sides Γ_+ (interfaces (k) and $(k+1)$) or Γ_- (interfaces $(k-1)$ and (k)). The eigenvalues and eigenvectors of $\widehat{\mathbf{S}}$ are usually denoted as μ_j and $\boldsymbol{\phi}_j$ (respectively) and are referred to as the wave modes of the periodic structure. The eigenvalues μ_j have the meaning of wave parameters defined so that $\mu_j = \mathtt{exp}(-\mathtt{i}\beta_j 2\Delta\theta)$ where β_j are circumferential wave numbers[1]. Also, the eigenvectors $\boldsymbol{\phi}_j$ represent the wave mode shapes. They are expressed by $\boldsymbol{\phi}_j = [\boldsymbol{\phi}_{\mathtt{q}j}^T \ \boldsymbol{\phi}_{\mathtt{F}j}^T]^T$, where $\boldsymbol{\phi}_{\mathtt{q}j}$ and $\boldsymbol{\phi}_{\mathtt{F}j}$ are $n \times 1$ vectors of displacement and force components.

Since the matrix $\widehat{\mathbf{S}}$ is symplectic, its eigenvalues come in pairs as μ_j and $1/\mu_j$. Also, since damping is taken into account in the modeling of the substructures, one has $|\mu_j| \neq 1$. This means that purely propagating waves are discarded in favor of slightly damped propagating waves. Evanescent and complex waves occur as well. As a rule of thumb, the eigensolutions of the matrix $\widehat{\mathbf{S}}$ are classified into n positive-going wave modes $(\mu_j, \boldsymbol{\phi}_j)$ — i.e., which travel around the positive circumferential direction — defined so that $|\mu_j| < 1$, and n negative-going wave modes $(\mu_j^\star, \boldsymbol{\phi}_j^\star)$ defined so that $\mu_j^\star = 1/\mu_j$, i.e., $|\mu_j^\star| > 1$.

2.3. Forced response

Within the WFE framework, the displacement/force vectors at coupling interfaces are expressed in terms of wave mode shapes as follows [23]:

$$\widehat{\mathbf{q}}_{\Gamma_+}^{(k)} = \widehat{\mathbf{q}}_{\Gamma_-}^{(k)} = \boldsymbol{\Phi}_{\mathtt{q}}\mathbf{Q}^{(k)} + \boldsymbol{\Phi}_{\mathtt{q}}^\star\mathbf{Q}^{\star(k)}, \tag{26}$$

$$\widehat{\mathbf{F}}_{\Gamma_+}^{(k)} = -\widehat{\mathbf{F}}_{\Gamma_-}^{(k)} = \boldsymbol{\Phi}_{\mathtt{F}}\mathbf{Q}^{(k)} + \boldsymbol{\Phi}_{\mathtt{F}}^\star\mathbf{Q}^{\star(k)}, \tag{27}$$

where $\boldsymbol{\Phi}_{\mathtt{q}} = [\boldsymbol{\phi}_{\mathtt{q}1} \cdots \boldsymbol{\phi}_{\mathtt{q}n}]$, $\boldsymbol{\Phi}_{\mathtt{q}}^\star = [\boldsymbol{\phi}_{\mathtt{q}1}^\star \cdots \boldsymbol{\phi}_{\mathtt{q}n}^\star]$, $\boldsymbol{\Phi}_{\mathtt{F}} = [\boldsymbol{\phi}_{\mathtt{F}1} \cdots \boldsymbol{\phi}_{\mathtt{F}n}]$ and $\boldsymbol{\Phi}_{\mathtt{F}}^\star = [\boldsymbol{\phi}_{\mathtt{F}1}^\star \cdots \boldsymbol{\phi}_{\mathtt{F}n}^\star]$ are $n \times n$ matrices of wave mode shapes. Also, $\mathbf{Q}^{(k)} = [Q_1^{(k)} \cdots Q_n^{(k)}]^T$ and $\mathbf{Q}^{\star(k)} = [Q_1^{\star(k)} \cdots Q_n^{\star(k)}]^T$ are vectors of wave amplitudes for the positive-going and negative-going wave modes. The vectors of wave amplitudes at two consecutive interfaces (k) and $(k+1)$ enclosing a non-excited substructure are displayed in Figure 2. They are linked as follows [14]:

$$\mathbf{Q}^{(k+1)} = \boldsymbol{\mu}\mathbf{Q}^{(k)} \quad , \quad \mathbf{Q}^{\star(k)} = \boldsymbol{\mu}\mathbf{Q}^{\star(k+1)}, \tag{28}$$

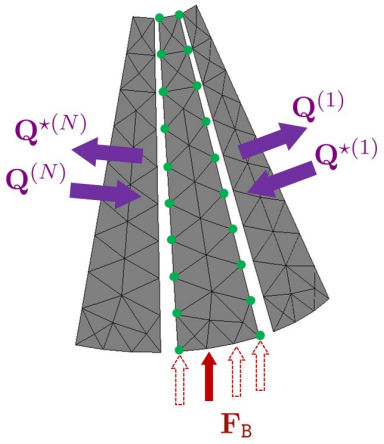

Figure 3: Vectors of wave amplitudes $\mathbf{Q}^{(1)}$, $\mathbf{Q}^{\star(1)}$, $\mathbf{Q}^{(N)}$ and $\mathbf{Q}^{\star(N)}$ at the coupling interfaces of the excited substructure.

where $\boldsymbol{\mu} = \mathtt{diag}\{\mu_j\}_j$ is the $n \times n$ diagonal matrix of the eigenvalues of $\widehat{\mathbf{S}}$ that concern the positive-going wave modes, i.e., those for which $|\mu_j| < 1$.

Consider the particular case of a periodic structure composed of N substructures, with one excited substructure and $N-1$ non-excited substructures. Hence, N coupling interfaces are to be considered, starting from (1) until (N) from the "right" to the "left" sides of the excited substructure as shown in Figure 3. Denote as $\mathbf{Q}$ and $\mathbf{Q}^{\star}$ the vectors of wave amplitudes at the right and left sides of the excited substructure, i.e.:

$$\mathbf{Q} = \mathbf{Q}^{(1)} \quad , \quad \mathbf{Q}^{\star} = \mathbf{Q}^{\star(N)}. \tag{29}$$

Hence, from Eq. (28), the vectors of wave amplitudes at an arbitrary interface (k) are expressed by:

$$\mathbf{Q}^{(k)} = \boldsymbol{\mu}^{k-1}\mathbf{Q} \quad , \quad \mathbf{Q}^{\star(k)} = \boldsymbol{\mu}^{N-k}\mathbf{Q}^{\star}. \tag{30}$$

Eq. (30) means that the displacement/force vectors at the substructure interface (k) (cf. Eqs. (26) and (27)) can be assessed from the knowledge of the vectors of wave amplitudes $\mathbf{Q}$ and $\mathbf{Q}^{\star}$. The determination of $\mathbf{Q}$ and $\mathbf{Q}^{\star}$ is achieved as follows. Let us rewrite Equation (9) in cylindrical coordinates by means of the transformation matrix $\mathcal{H}$, Eq. (20). This gives

$$\widehat{\mathbf{D}}^{*} \begin{bmatrix} \widehat{\mathbf{q}}^{(N)}_{\Gamma_-} \\ \widehat{\mathbf{q}}^{(1)}_{\Gamma_+} \end{bmatrix} = \begin{bmatrix} \widehat{\mathbf{F}}^{(N)}_{\Gamma_-} \\ \widehat{\mathbf{F}}^{(1)}_{\Gamma_+} \end{bmatrix} + \mathcal{H}\boldsymbol{\Theta}_{\Gamma\mathtt{B}}\mathbf{F}_{\mathtt{B}}, \tag{31}$$

where

$$\boldsymbol{\Theta}_{\Gamma\mathtt{B}} = \mathcal{L}_{\Gamma\mathtt{B}} + (\mathbf{X}^{T}_{\mathtt{st}} - \widetilde{\mathbf{D}}_{\mathtt{st-el}}\widetilde{\mathbf{D}}^{-1}_{\mathtt{el-el}}\widetilde{\mathbf{X}}^{T}_{\mathtt{el}})\mathcal{L}_{\mathtt{IB}}. \tag{32}$$

From Eqs. (26), (27) and (30), one has:

$$\widehat{\mathbf{q}}^{(N)}_{\Gamma_-} = \boldsymbol{\Phi}_{\mathtt{q}}\boldsymbol{\mu}^{N-1}\mathbf{Q} + \boldsymbol{\Phi}^{\star}_{\mathtt{q}}\mathbf{Q}^{\star} \quad , \quad \widehat{\mathbf{q}}^{(1)}_{\Gamma_+} = \boldsymbol{\Phi}_{\mathtt{q}}\mathbf{Q} + \boldsymbol{\Phi}^{\star}_{\mathtt{q}}\boldsymbol{\mu}^{N-1}\mathbf{Q}^{\star}, \tag{33}$$

$$\widehat{\mathbf{F}}^{(N)}_{\Gamma_-} = -\boldsymbol{\Phi}_{\mathtt{F}}\boldsymbol{\mu}^{N-1}\mathbf{Q} - \boldsymbol{\Phi}^{\star}_{\mathtt{F}}\mathbf{Q}^{\star} \quad , \quad \widehat{\mathbf{F}}^{(1)}_{\Gamma_+} = \boldsymbol{\Phi}_{\mathtt{F}}\mathbf{Q} + \boldsymbol{\Phi}^{\star}_{\mathtt{F}}\boldsymbol{\mu}^{N-1}\mathbf{Q}^{\star}. \tag{34}$$

[1]The circumferential wave numbers are defined as $\beta_j = \omega/c_{\mathtt{a}j}$ where $c_{\mathtt{a}j}$ are the angular wave velocities. Note that, within the present framework, the circumferential wave numbers are complex and can have arbitrary values, which particularly means that the terms $\beta_j 2\Delta\theta$ are not restricted to multiples of $2\pi/N$.

As a result, Eq. (31) leads to

$$\widehat{\mathbf{D}}^{*}\begin{bmatrix}\boldsymbol{\Phi}_{\mathtt{q}}\boldsymbol{\mu}^{N-1} & \boldsymbol{\Phi}_{\mathtt{q}}^{\star}\\ \boldsymbol{\Phi}_{\mathtt{q}} & \boldsymbol{\Phi}_{\mathtt{q}}^{\star}\boldsymbol{\mu}^{N-1}\end{bmatrix}\begin{bmatrix}\mathbf{Q}\\ \mathbf{Q}^{\star}\end{bmatrix}=\begin{bmatrix}-\boldsymbol{\Phi}_{\mathtt{F}}\boldsymbol{\mu}^{N-1} & -\boldsymbol{\Phi}_{\mathtt{F}}^{\star}\\ \boldsymbol{\Phi}_{\mathtt{F}} & \boldsymbol{\Phi}_{\mathtt{F}}^{\star}\boldsymbol{\mu}^{N-1}\end{bmatrix}\begin{bmatrix}\mathbf{Q}\\ \mathbf{Q}^{\star}\end{bmatrix}+\mathcal{H}\boldsymbol{\Theta}_{\Gamma\mathtt{B}}\mathbf{F}_{\mathtt{B}}. \tag{35}$$

Eq. (35) may be simplified as follows (see Appendix):

$$(\widehat{\mathbf{D}}^{*}\boldsymbol{\Psi}_{\mathtt{q}}-\boldsymbol{\Psi}_{\mathtt{F}})\begin{bmatrix}\mathbf{0} & \mathbf{I}_n-\boldsymbol{\mu}^{N}\\ \mathbf{I}_n-\boldsymbol{\mu}^{N} & \mathbf{0}\end{bmatrix}\begin{bmatrix}\mathbf{Q}\\ \mathbf{Q}^{\star}\end{bmatrix}=\mathcal{H}\boldsymbol{\Theta}_{\Gamma\mathtt{B}}\mathbf{F}_{\mathtt{B}}, \tag{36}$$

where

$$\boldsymbol{\Psi}_{\mathtt{q}}=\begin{bmatrix}\boldsymbol{\Phi}_{\mathtt{q}}^{\star} & \mathbf{0}\\ \mathbf{0} & \boldsymbol{\Phi}_{\mathtt{q}}\end{bmatrix}\quad,\quad\boldsymbol{\Psi}_{\mathtt{F}}=\begin{bmatrix}-\boldsymbol{\Phi}_{\mathtt{F}}^{\star} & \mathbf{0}\\ \mathbf{0} & \boldsymbol{\Phi}_{\mathtt{F}}\end{bmatrix}. \tag{37}$$

Solving Eq. (36) finally yields the vectors of wave amplitudes $\mathbf{Q}$ and $\mathbf{Q}^{\star}$, i.e.:

$$\begin{bmatrix}\mathbf{Q}\\ \mathbf{Q}^{\star}\end{bmatrix}=\begin{bmatrix}\mathbf{0} & (\mathbf{I}_n-\boldsymbol{\mu}^{N})^{-1}\\ (\mathbf{I}_n-\boldsymbol{\mu}^{N})^{-1} & \mathbf{0}\end{bmatrix}(\widehat{\mathbf{D}}^{*}\boldsymbol{\Psi}_{\mathtt{q}}-\boldsymbol{\Psi}_{\mathtt{F}})^{-1}\mathcal{H}\boldsymbol{\Theta}_{\Gamma\mathtt{B}}\mathbf{F}_{\mathtt{B}}. \tag{38}$$

The determination of the displacement/force vectors at coupling interfaces follows from Eq. (30), and Eqs. (26-27).

2.4. Dynamic flexibility modes

Define the following displacement vector of a non-excited substructure enclosed between two interfaces (k) and $(k+1)$, expressed in the local cartesian coordinate system of this substructure:

$$\mathbf{q}^{(k)}=\begin{bmatrix}\mathbf{q}_{\Gamma_-}^{(k)}\\ \mathbf{q}_{\mathtt{I}|\mathtt{B}}^{(k)}\end{bmatrix}\qquad k=1,\cdots,N-1, \tag{39}$$

where $\mathbf{q}_{\Gamma_-}^{(k)}$ is the displacement vector at the interface Γ_-, and $\mathbf{q}_{\mathtt{I}|\mathtt{B}}^{(k)}$ is the displacement vector of the internal DOFs which are restricted to the boundary of the substructure (see Figure 3). The latter is expressed by $\mathbf{q}_{\mathtt{I}|\mathtt{B}}\approx\mathbf{X}_{\mathtt{st}|\mathtt{B}}\mathbf{q}_{\Gamma}+\widetilde{\mathbf{X}}_{\mathtt{el}|\mathtt{B}}\widetilde{\boldsymbol{\alpha}}$ (see Eq. (4)), where $\mathbf{q}_{\Gamma}$ is given by $\mathbf{q}_{\Gamma}=[(\mathbf{q}_{\Gamma_-}^{(k)})^{T}(\mathbf{q}_{\Gamma_-}^{(k+1)})^{T}]^{T}$, and $\widetilde{\boldsymbol{\alpha}}$ is given by Eq. (8) with $\mathbf{F}_{\mathtt{B}}=\mathbf{0}$. As a result, the displacement vector $\mathbf{q}^{(k)}$ is expressed by

$$\begin{bmatrix}\mathbf{q}_{\Gamma_-}^{(k)}\\ \mathbf{q}_{\mathtt{I}|\mathtt{B}}^{(k)}\end{bmatrix}=\begin{bmatrix}[\mathbf{I}_n & \mathbf{0}]\\ \mathbf{X}_{\mathtt{st}|\mathtt{B}}-\widetilde{\mathbf{X}}_{\mathtt{el}|\mathtt{B}}\widetilde{\mathbf{D}}_{\mathtt{el}-\mathtt{el}}^{-1}\widetilde{\mathbf{D}}_{\mathtt{st}-\mathtt{el}}^{T}\end{bmatrix}\begin{bmatrix}\mathbf{q}_{\Gamma_-}^{(k)}\\ \mathbf{q}_{\Gamma_-}^{(k+1)}\end{bmatrix}. \tag{40}$$

Expressing the displacement vectors $\mathbf{q}_{\Gamma_-}^{(k)}$ and $\mathbf{q}_{\Gamma_-}^{(k+1)}$ on the right hand side of Eq. (40) in cylindrical coordinates gives[2]:

$$\begin{bmatrix}\mathbf{q}_{\Gamma_-}^{(k)}\\ \mathbf{q}_{\mathtt{I}|\mathtt{B}}^{(k)}\end{bmatrix}=\begin{bmatrix}[\mathbf{I}_n & \mathbf{0}]\\ \mathbf{X}_{\mathtt{st}|\mathtt{B}}-\widetilde{\mathbf{X}}_{\mathtt{el}|\mathtt{B}}\widetilde{\mathbf{D}}_{\mathtt{el}-\mathtt{el}}^{-1}\widetilde{\mathbf{D}}_{\mathtt{st}-\mathtt{el}}^{T}\end{bmatrix}\mathcal{H}^{T}\begin{bmatrix}\widehat{\mathbf{q}}_{\Gamma_-}^{(k)}\\ \widehat{\mathbf{q}}_{\Gamma_-}^{(k+1)}\end{bmatrix}. \tag{41}$$

Finally, from Eqs. (26) and (30), one has:

$$\begin{bmatrix}\mathbf{q}_{\Gamma_-}^{(k)}\\ \mathbf{q}_{\mathtt{I}|\mathtt{B}}^{(k)}\end{bmatrix}=\begin{bmatrix}[\mathbf{I}_n & \mathbf{0}]\\ \mathbf{X}_{\mathtt{st}|\mathtt{B}}-\widetilde{\mathbf{X}}_{\mathtt{el}|\mathtt{B}}\widetilde{\mathbf{D}}_{\mathtt{el}-\mathtt{el}}^{-1}\widetilde{\mathbf{D}}_{\mathtt{st}-\mathtt{el}}^{T}\end{bmatrix}\mathcal{H}^{T}\begin{bmatrix}\boldsymbol{\Phi}_{\mathtt{q}}\boldsymbol{\mu}^{k-1} & \boldsymbol{\Phi}_{\mathtt{q}}^{\star}\boldsymbol{\mu}^{N-k}\\ \boldsymbol{\Phi}_{\mathtt{q}}\boldsymbol{\mu}^{k} & \boldsymbol{\Phi}_{\mathtt{q}}^{\star}\boldsymbol{\mu}^{N-k-1}\end{bmatrix}\begin{bmatrix}\mathbf{Q}\\ \mathbf{Q}^{\star}\end{bmatrix}, \tag{42}$$

[2] See Eq. (19), where $\mathbf{q}_{\Gamma_+}^{(k+1)}=\mathbf{q}_{\Gamma_-}^{(k+1)}$ and $\mathcal{H}^{-1}=\mathcal{H}^{T}$.

where $\mathbf{Q}$ and $\mathbf{Q}^\star$ are the vectors of wave amplitudes, Eq. (38).

On the other hand, by considering the excited substructure — i.e., the one between the interfaces (N) and (1) where $\mathbf{F}_{\mathtt{B}} \neq \mathbf{0}$ —, Eq. (42) is to be written as[3]:

$$\mathbf{q}^{(N)} = \begin{bmatrix} \mathbf{q}^{(N)}_{\Gamma_-} \\ \mathbf{q}^{(N)}_{\mathtt{I|B}} \end{bmatrix} = \begin{bmatrix} [\mathbf{I}_n \quad \mathbf{0}] \\ \mathbf{X}_{\mathtt{st|B}} - \widetilde{\mathbf{X}}_{\mathtt{el|B}} \widetilde{\mathbf{D}}^{-1}_{\mathtt{el-el}} \widetilde{\mathbf{D}}^{T}_{\mathtt{st-el}} \end{bmatrix} \mathcal{H}^T \begin{bmatrix} \mathbf{\Phi}_{\mathtt{q}} \boldsymbol{\mu}^{k-1} & \mathbf{\Phi}^\star_{\mathtt{q}} \boldsymbol{\mu}^{N-k} \\ \mathbf{\Phi}_{\mathtt{q}} \boldsymbol{\mu}^{k} & \mathbf{\Phi}^\star_{\mathtt{q}} \boldsymbol{\mu}^{N-k-1} \end{bmatrix} \begin{bmatrix} \mathbf{Q} \\ \mathbf{Q}^\star \end{bmatrix} + \begin{bmatrix} \mathbf{0} \\ \widetilde{\mathbf{X}}_{\mathtt{el|B}} \widetilde{\mathbf{D}}^{-1}_{\mathtt{el-el}} \widetilde{\mathbf{X}}^{T}_{\mathtt{el}} \mathcal{L}_{\mathtt{IB}} \end{bmatrix} \mathbf{F}_{\mathtt{B}}. \tag{43}$$

Finally, the displacement vector of the whole periodic structure can be defined as follows:

$$\mathbf{q} = \begin{bmatrix} (\mathbf{I}_{(n+n_{\mathtt{I|B}})/3} \otimes \mathcal{R}) \mathbf{q}^{(1)} \\ (\mathbf{I}_{(n+n_{\mathtt{I|B}})/3} \otimes \mathcal{R}^2) \mathbf{q}^{(2)} \\ \vdots \\ (\mathbf{I}_{(n+n_{\mathtt{I|B}})/3} \otimes \mathcal{R}^N) \mathbf{q}^{(N)} \end{bmatrix}, \tag{44}$$

where $n_{\mathtt{I|B}}$ is the number of internal DOFs which belong to the boundary of a substructure (see Figure 1), and $\mathcal{R} = \mathcal{R}_{-2\Delta\theta}$ is a 3×3 rotation matrix, with $\mathcal{R}^k = \mathcal{R} \times \cdots \times \mathcal{R}$ and $\mathcal{R}^N = \mathbf{I}_3$, whose purpose is to express the displacement vector of each substructure in the global cartesian reference system of the periodic structure. In the present case, the global cartesian coordinate system is chosen so that it matches the local cartesian coordinate system of the excited substructure.

To sum up, the displacement vector $\mathbf{q}$ of the periodic structure can be expressed via the WFE method. This requires the vectors of wave amplitudes $\mathbf{Q}$ and $\mathbf{Q}^\star$ to be computed first by considering the methodology proposed in Section 2.3. The displacement vector $\mathbf{q}$ represents the dynamic response of the structure subject to a unit force at the boundary DOF i of the substructure enclosed between the interfaces (N) and (1) (see Figure 1). This is defined as the dynamic flexibility mode $\mathbf{q} \rightarrow \boldsymbol{\chi}^{(N)}_i$. By scanning all the boundary DOFs of the substructure — i.e., all the state of excitations i —, except those on the interface Γ_+ which will be part of the next substructure, the following matrix of dynamic flexibility modes can be formulated:

$$\mathbf{X}^{(N)} = [\boldsymbol{\chi}^{(N)}_1 \boldsymbol{\chi}^{(N)}_2 \cdots \boldsymbol{\chi}^{(N)}_{n_{\mathtt{B}}}], \tag{45}$$

where $n_{\mathtt{B}}$ is the number of boundary nodes of the substructure (except those on Γ_+). Therefore, the displacement vector of the whole structure which results from a vector of boundary forces $\mathbf{F}^{(N)}_{\mathtt{B}}$ applied to the substructure enclosed between the interfaces (N) and (1), is given by:

$$\mathbf{q} = \mathbf{X}^{(N)} \mathbf{F}^{(N)}_{\mathtt{B}}. \tag{46}$$

Eq. (46) is nothing but the well-known superposition principle in linear mechanics.

The matrix of dynamic flexibility modes $\mathbf{X}^{(k)}$ which concerns an excited substructure enclosed between two arbitrary interfaces (k) and $(k+1)$, instead of (N) and (1), is obtained as follows. Apply a permutation matrix $\mathcal{P}^{(k)}$ and a rotation matrix $\mathcal{R}^k$ to the displacement vector $\mathbf{q}$ in Eq. (44):

$$\mathbf{q} \rightarrow (\mathbf{I}_{n_{\mathtt{T}}/3} \otimes \mathcal{R}^k) \mathcal{P}^{(k)} \mathbf{q} = (\mathbf{I}_{n_{\mathtt{T}}/3} \otimes \mathcal{R}^k) \begin{bmatrix} (\mathbf{I}_{(n+n_{\mathtt{I|B}})/3} \otimes \mathcal{R}^{N-k+1}) \mathbf{q}^{(N-k+1)} \\ \vdots \\ (\mathbf{I}_{(n+n_{\mathtt{I|B}})/3} \otimes \mathcal{R}^{N}) \mathbf{q}^{(N)} \\ (\mathbf{I}_{(n+n_{\mathtt{I|B}})/3} \otimes \mathcal{R}) \mathbf{q}^{(1)} \\ \vdots \\ (\mathbf{I}_{(n+n_{\mathtt{I|B}})/3} \otimes \mathcal{R}^{N-k}) \mathbf{q}^{(N-k)} \end{bmatrix}, \tag{47}$$

[3] in this case, $\widetilde{\boldsymbol{\alpha}}$ is given by Eq. (8) with $\mathbf{F}_{\mathtt{B}} \neq \mathbf{0}$.

where $n_{\mathtt{T}} = N(n + n_{\mathtt{I|B}})$. Also, apply a rotation matrix $\mathcal{R}^k$ to the vector of boundary forces $\mathbf{F}_{\mathtt{B}}^{(N)}$:

$$\mathbf{F}_{\mathtt{B}}^{(k)} = (\mathbf{I}_{n_{\mathtt{B}}/3} \otimes \mathcal{R}^k)\mathbf{F}_{\mathtt{B}}^{(N)}. \tag{48}$$

Eqs. (47) and (48) yield the following matrix of dynamic flexibility modes:

$$\mathbf{X}^{(k)} = (\mathbf{I}_{n_{\mathtt{T}}/3} \otimes \mathcal{R}^k)\mathcal{P}^{(k)}\mathbf{X}^{(N)}(\mathbf{I}_{n_{\mathtt{B}}/3} \otimes \mathcal{R}^k)^T. \tag{49}$$

Hence, the matrix of dynamic flexibility modes of the whole periodic structure can be written as:

$$\mathbf{X} = [\mathbf{X}^{(1)}\mathbf{X}^{(2)} \cdots \mathbf{X}^{(N)}]. \tag{50}$$

By considering the matrix of dynamic flexibility modes, the displacement vector of the periodic structure which results from an arbitrary vector of boundary forces $\mathbf{F}_{\mathtt{B}}$ can be computed as follows: $\mathbf{q} = \mathbf{X}\mathbf{F}_{\mathtt{B}}$.

The interesting feature of the proposed approach is that the computation of the matrix of dynamic flexibility modes is not cumbersome, for a twofold reason:

- CB method: this enables the condensed DSM of a substructure (matrix $\mathbf{D}^*$, Eq. (10)) and the matrix $\mathbf{\Theta}_{\Gamma\mathtt{B}}$ (Eq. (32)) to be quickly computed, i.e., when compared to the classic way consisting in inverting the whole DSM of the internal DOFs of the substructure. Also, the first matrix term in Eqs. (42) and (43), and the last matrix term in Eq. (43), involve small-sized matrix products which are not computationally cumbersome.
- WFE method: this enables the displacement vectors at the substructure interfaces to be quickly computed. The reason lies in the consideration of a small-sized matrix equation (size $2n \times 2n$) to compute the vectors of wave amplitudes $\mathbf{Q}$ and $\mathbf{Q}^\star$ (see Eq. (36)), and the use of a $n \times n$ diagonal matrix $\boldsymbol{\mu}$ in Eqs. (42) and (43) whose powers ($\boldsymbol{\mu}^{k-1}$, $\boldsymbol{\mu}^{N-k}$, ...) can be easily determined.

Remark 1. The displacement vector $\mathbf{q}$ concerns the interface DOFs and the boundary DOFs of the periodic structure. Computing the displacement vector at the internal DOFs of an arbitrary substructure requires one to consider the static modes and fixed interface modes of the substructure (see after Eq. (3)). This gives:

$$\mathbf{q}_{\mathtt{I}} \approx (\mathbf{I}_{n_{\mathtt{T}}/3} \otimes \mathcal{R}^k)\left(\mathbf{X}_{\mathtt{st}}(\mathbf{I}_{2n/3} \otimes \mathcal{R}^k)^T\mathbf{q}_\Gamma + \widetilde{\mathbf{X}}_{\mathtt{el}}\widetilde{\boldsymbol{\alpha}}\right), \tag{51}$$

where

$$\widetilde{\boldsymbol{\alpha}} = \widetilde{\mathbf{D}}_{\mathtt{el-el}}^{-1}\left(\widetilde{\mathbf{X}}_{\mathtt{el}}^T\mathcal{L}_{\mathtt{IB}}(\mathbf{I}_{n_{\mathtt{B}}/3} \otimes \mathcal{R}^k)^T\mathbf{F}_{\mathtt{B}} - \widetilde{\mathbf{D}}_{\mathtt{st-el}}^T(\mathbf{I}_{n_{\mathtt{I}}/3} \otimes \mathcal{R}^k)^T\mathbf{q}_\Gamma\right). \tag{52}$$

Remark 2. The size of the matrix of dynamic flexibility modes $\mathbf{X}$ is $n_{\mathtt{T}} \times n_{\mathtt{TB}}$ where $n_{\mathtt{T}}$ is the total number of interface and boundary DOFs of the structure, and $n_{\mathtt{TB}} = Nn_{\mathtt{B}}$ is the total number of boundary DOFs. It is reasonable to assume that $n_{\mathtt{TB}}$ is small compared to $n_{\mathtt{T}}$, which means that the total number of boundary DOFs — i.e. where excitations and coupling conditions are supposed to occur — is small compared to the total number of interface DOFs. In other words, the matrices of dynamic flexibility modes of periodic structures represent rectangular matrices with a small column size. Therefore, they can be quickly built and assembled together to model assemblies made up of several periodic structures.

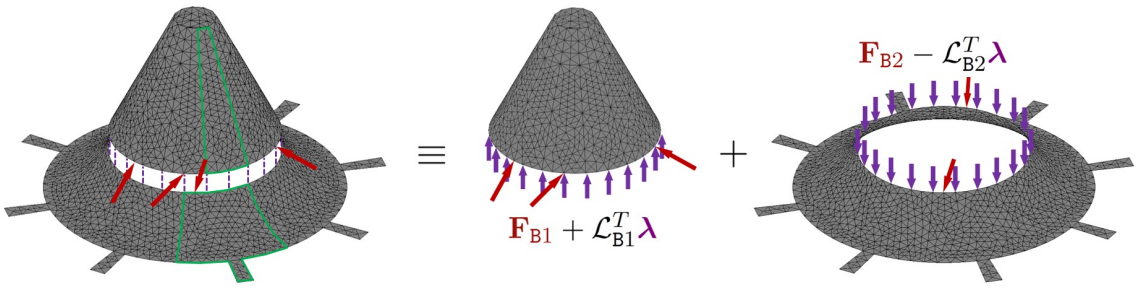

Figure 4: FE meshes of two periodic structures which are connected together and subject to boundary forces.

2.5. Dynamic substructuring

Consider for the sake of clarity two periodic structures 1 and 2 which are connected together as shown in Figure 4, on several boundary DOFs. Denote as $\boldsymbol{\lambda}$ the vector of coupling forces, and denote as $\mathbf{F}_{B1}$ and $\mathbf{F}_{B2}$ the vectors of external forces which are applied to the boundary DOFs of structures 1 and 2, respectively. As a whole, the vectors of boundary forces are defined as $\mathbf{F}_{B1} + \mathcal{L}_{B1}^T \boldsymbol{\lambda}$ and $\mathbf{F}_{B2} - \mathcal{L}_{B2}^T \boldsymbol{\lambda}$ (Figure 4) where $\mathcal{L}_{B1}$ and $\mathcal{L}_{B2}$ are Boolean matrices which localize the coupling DOFs among the boundary DOFs of periodic structures 1 and 2, respectively.

Denote as $\mathbf{q}_1$ and $\mathbf{q}_2$ the displacement vectors of structures 1 and 2, respectively. Hence, by considering the matrices of dynamic flexibility modes $\mathbf{X}_1$ and $\mathbf{X}_2$ of the periodic structures, $\mathbf{q}_1$ and $\mathbf{q}_2$ can be expressed as follows:

$$\mathbf{q}_1 = \mathbf{X}_1(\mathbf{F}_{B1} + \mathcal{L}_{B1}^T \boldsymbol{\lambda}) \quad , \quad \mathbf{q}_2 = \mathbf{X}_2(\mathbf{F}_{B2} - \mathcal{L}_{B2}^T \boldsymbol{\lambda}). \tag{53}$$

On the other hand, the coupling conditions yield:

$$\mathcal{L}_1 \mathbf{q}_1 - \mathcal{L}_2 \mathbf{q}_2 = \mathbf{0}, \tag{54}$$

where $\mathcal{L}_1$ and $\mathcal{L}_2$ are Boolean localization matrices. Eqs. (53) and (54) lead to the following matrix equation:

$$\begin{bmatrix} \mathbf{I} & \mathbf{0} & -\mathbf{X}_1 \mathcal{L}_{B1}^T \\ \mathbf{0} & \mathbf{I} & \mathbf{X}_2 \mathcal{L}_{B2}^T \\ \mathcal{L}_1 & -\mathcal{L}_2 & \mathbf{0} \end{bmatrix} \begin{bmatrix} \mathbf{q}_1 \\ \mathbf{q}_2 \\ \boldsymbol{\lambda} \end{bmatrix} = \begin{bmatrix} \mathbf{X}_1 \mathbf{F}_{B1} \\ \mathbf{X}_2 \mathbf{F}_{B2} \\ \mathbf{0} \end{bmatrix}. \tag{55}$$

Solving Eq. (55) yields:

$$\boldsymbol{\lambda} = -(\mathcal{L}_1 \mathbf{X}_1 \mathcal{L}_{B1}^T + \mathcal{L}_2 \mathbf{X}_2 \mathcal{L}_{B2}^T)^{-1} (\mathcal{L}_1 \mathbf{X}_1 \mathbf{F}_{B1} - \mathcal{L}_2 \mathbf{X}_2 \mathbf{F}_{B2}). \tag{56}$$

Notice that the computation of the vector $\boldsymbol{\lambda}$ is not cumbersome. First, Eq. (56) does not require the inversion of the DSMs of the structures as this is commonly done in domain decomposition technique [24]; also, $\mathbf{X}_1$ and $\mathbf{X}_2$ are small column size matrices (see Remark 2 at the end of Section 2.4) which can be easily multiplied with other matrices and vectors.

The determination of the displacement vectors $\mathbf{q}_1$ and $\mathbf{q}_2$ follows from Eq. (53).

The analysis of assemblies made up of three or more periodic structures can be achieved through simple adaptations of the proposed strategy. Also, the consideration of periodic structures coupled with non-periodic structures can be investigated without any additional difficulty. The strategy consists in expressing the matrices of dynamic flexibility modes of the structures, and connecting these by considering the proposed procedure.

3. Numerical results

The relevance of the proposed approach is discussed through three study cases: (i) a single periodic structure with $N = 36$ substructures, named structure P36 (Figure 5); (ii) an assembly made up of a structure P36 and

a structure with $N_2 = 60$ substructures (structure P60) (Figure 8); (iii) an assembly made up of two similar structures P36 and a third structure P60 (Figure 14). For each structure, the boundary DOFs considered are those located on the inner circumferential surface. The global dimensions of the substructures are displayed in Figures 5 and 8. The structures P36 and P60 have the same material properties, i.e., a density of 7800 kg/m^3, a Young's modulus of 2.1×10^{11} Pa, a Poisson's ratio of 0.3, and a loss factor of 5×10^{-3}. The substructures are meshed using four node tetrahedral elements, with three translational DOFs per node. Hence, concerning structure P36 (Figure 5), 3786 DOFs are used to mesh each substructure; concerning structure P60 (Figure 8), 1746 DOFs are used. Also, $n_1 = 84$ and $n_2 = 117$ DOFs are used to mesh the substructure interfaces for structures P36 and P60, respectively. The structure (P36) in Figure 5 and the structural assemblies in Figures 8 and 14 are excited in the same way by considering four pairs of point forces of same magnitude acting along the circumferential direction, at $\theta = 0^o$, $\theta = 90^o$, $\theta = 180^o$ and $\theta = 270^o$, on the boundary DOFs of the structure P36 as shown in Figure 5. Regarding Figure 14, only the second structure P36 is excited. For each test case, the transverse displacement ($x-$direction) of the excited structure P36 is analyzed at one measurement point as shown in Figure 5. Hence, the frequency response functions (FRFs) are analyzed over a frequency band of $[0 \text{ Hz}\,,\ 5000 \text{ Hz}]$ which is done by considering a sample of 1000 discrete frequencies which are equally spaced with a frequency step of 5 Hz.

Note that, within the CB framework (Section 2.1), 20 fixed interface modes are considered to compute the condensed DSMs of the substructures. This number meets the criterion mentioned before Eq. (5), and has been confirmed through a sensitivity analysis.

The proposed (WFE) approach is compared with the FE method. Comparisons with the theory of cyclic symmetry [2, 3, 25] are also performed regarding the first two cases. It should be emphasized that, within the framework of the theory of cyclic symmetry, the displacement vectors of the substructures are expressed in terms of Fourier (harmonic) modes (see [2, 25]). By projecting the DSM of a whole periodic structure onto the space of Fourier modes, a set of uncoupled reduced matrix equations (for the substructures) can be expressed which can be quickly solved. This interesting feature follows from the orthogonality properties between the Fourier modes of a periodic structure. Problems arise for modeling assemblies made up of two or more periodic structures with different numbers of substructures and then, different Fourier modes which are not orthogonal to each other. In this case, coupling occurs between the harmonic modes of the structures, i.e., the matrix equation which models a structural assembly cannot be reduced in the same way as in the single structure case. To solve this issue, the assumption is therefore made to neglect the coupling between the Fourier/harmonic modes whose nodal diameters are different [3]. In other words, only the harmonics with the same nodal diameters are coupled together.

To further highlight the relevance of the WFE approach, an additional study case is considered consisting of an assembly made up of two structures (P36 and P60) with more DOFs as shown in Figure 11. In this case, the substructures involved in P36 and P60 are meshed with 7482 and 4878 DOFs, respectively, while $n_1 = 216$ and $n_2 = 315$ DOFs are used to describe the substructure interfaces, i.e., about three times the numbers of DOFs used in the previous test case (Figure 8). Again, four pairs of point forces acting along the circumferential direction of structure P36 are considered as shown in Figure 5. However, in the present case, the magnitudes of the forces are slightly perturbed — i.e., $+10\%$ and $+20\%$ for the locations $\theta = 90^o$ and $\theta = 180^o$, respectively — which breaks the cyclically symmetry properties of the excitation conditions and therefore adds complexities to the previous test case. Moreover, the FRF of the assembly is analyzed over an extended frequency band of $[0 \text{ Hz}\,,\ 10000 \text{ Hz}]$ (1000 discrete frequencies) with a view to highlighting the complex dynamics at high frequencies. In this case, 50 fixed interface modes are considered to compute the condensed DSMs of the substructures.

Each approach (WFE, FE, cyclic symmetry) is implemented using MATLAB® and simulated using an Intel® Xeon® CPU E3-1505M 3GHz processor. In order to precisely identify the drawbacks and advantages of each approach, the condensed DSMs $\mathbf{D}^*$ of the substructures (Eq. (10)) are considered in implementing each of the three approaches. The numerical impact of this choice on the efficiency of the FE method and the theory of cyclic symmetry is not strong however, keeping in mind that the condensation of the DSM of a substructure

is to be performed once for a given periodic structure, and leads to small matrix systems which can be solved more efficiently compared to the case when the full DSMs of the substructures are used. In this framework, the numerical tasks involved in the FE method consist of assembling the condensed DSMs of all the substructures in order to build the whole DSM of a periodic structure, and assembling the DSMs of the periodic structures in order to build the DSM of a structural assembly (Figures 8 and 14). On the other hand, the theory of cyclic symmetry involves considering a discrete Fourier transform [2] of the DSM of a periodic structure, as built from the condensed DSMs of the substructures.

3.1. Single periodic structure

Consider first a structure P36 as shown in Figure 5. Recall that the FE mesh of each substructure is composed of 3786 DOFs, and that each substructure interface (either Γ_+ or Γ_-) is described with $n = 84$ DOFs. The boundary DOFs of the periodic structure, i.e., where excitations can occur, are those located on the inner circumferential surface (see Figure 5). The boundary DOFs which are considered to model the substructures (see Section 2.4) are highlighted in red spots in Figure 5.

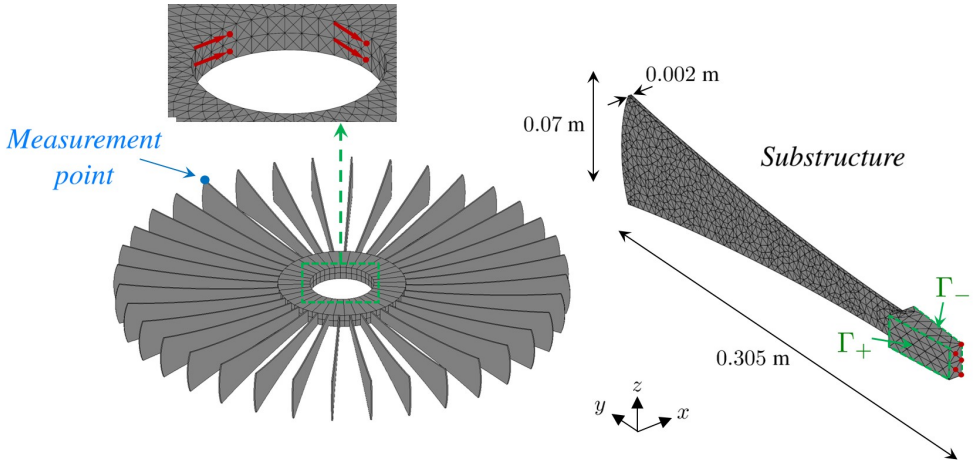

Figure 5: Periodic structure with 36 substructures (left), and FE mesh of a substructure (right); (red spots) boundary DOFs of the substructures.

The FRFs of the periodic structure issued from the WFE approach and the FE method are highlighted in Figure 6. Within the framework of the WFE approach, the displacement vector of the structure is computed as follows: $\mathbf{q} = \mathbf{X}\mathbf{F}_{\mathrm{B}}$ where $\mathbf{X}$ is the matrix of dynamic flexibility modes and $\mathbf{F}_{\mathrm{B}}$ is the vector of boundary forces. Also, a comparison between the theory of cyclic symmetry and the FE method is proposed in Figure 7. It is seen that both the WFE approach and the theory of cyclic symmetry are in perfect agreement with the FE method.

The CPU times involved in these three numerical approaches are listed in Table 1. It is seen that the WFE approach is about three times faster than the FE method. Also, the theory of cyclic symmetry appears to be more efficient than the FE method even compared to the WFE approach. In fact, the main advantage of the WFE approach, compared to the theory of cyclic symmetry, concerns the analysis of coupled systems. This will be clearly demonstrated in the next subsection.

Table 1: CPU times involved (one structure).

Approach used	CPU time	Reduction
FE	367 s	
WFE	135 s	63%
Cyclic	77 s	79%

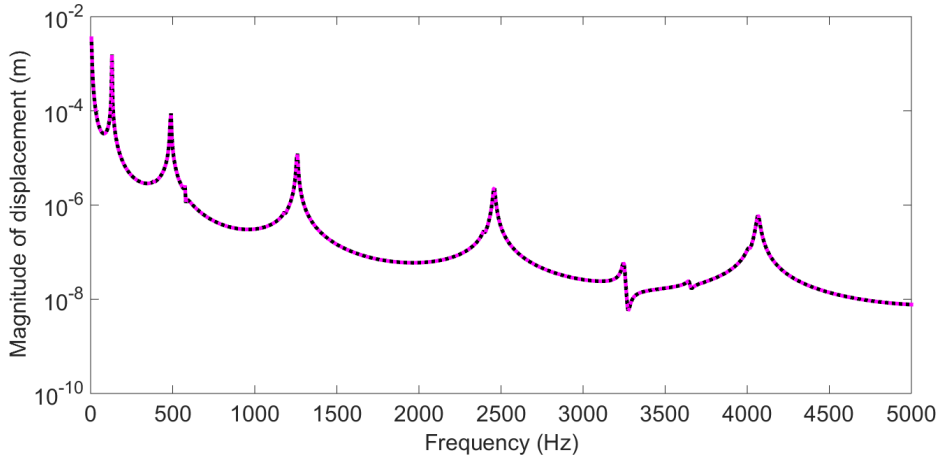

Figure 6: FRF of the periodic structure with 36 substructures: (black solid line) FE method; (pink dotted line) WFE approach.

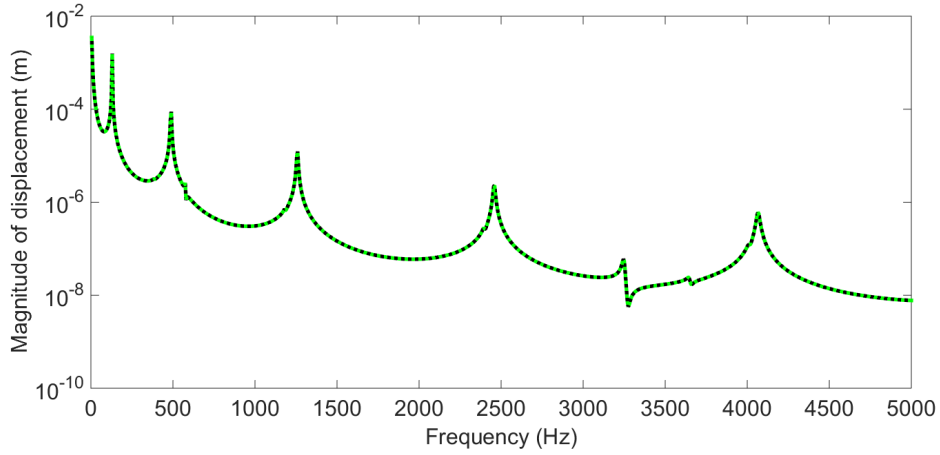

Figure 7: FRF of the periodic structure with 36 substructures: (black solid line) FE method; (green dotted line) theory of cyclic symmetry.

3.2. Two periodic structures

Consider now the case of a structure P36 coupled on part of its boundary with a structure P60 as shown in Figure 8. Concerning the structure P60, 1746 DOFs are used to model each substructure, while $n_2 = 117$ DOFs are used to discretize each substructure interface. The structures P36 and P60 are coupled on twelve nodes which are periodically distributed around their inner circumferential surfaces as shown in Figure 8 in red dashed lines, where the continuity of the displacements about the x, y and z directions is assumed.

Again, comparisons are carried out between the WFE approach and the FE method, and between the theory of cyclic theory and the FE method, as shown in Figures 9 and 10. Again, the accuracy of the WFE approach can be highlighted over the whole frequency range, without any ambiguity. In contrast, the theory of cyclic symmetry appears inaccurate for predicting the dynamic response of the structural assembly especially above 2500 Hz where large errors occur. The drawback of the theory of cyclic symmetry comes from the fact that the coupling between the harmonic modes of the periodic structures is neglected [3]. As it turns out, the potential of the theory of cyclic symmetry to tackle more complex problems — i.e., assemblies made up of several periodic structures — is jeopardized, i.e., large errors are expected when expressing the dynamic behavior of such systems.

The CPU times involved in the FE method, the WFE approach and the theory of cyclic symmetry are displayed in Table 2. It is shown that the WFE approach works much better than the FE method even compared

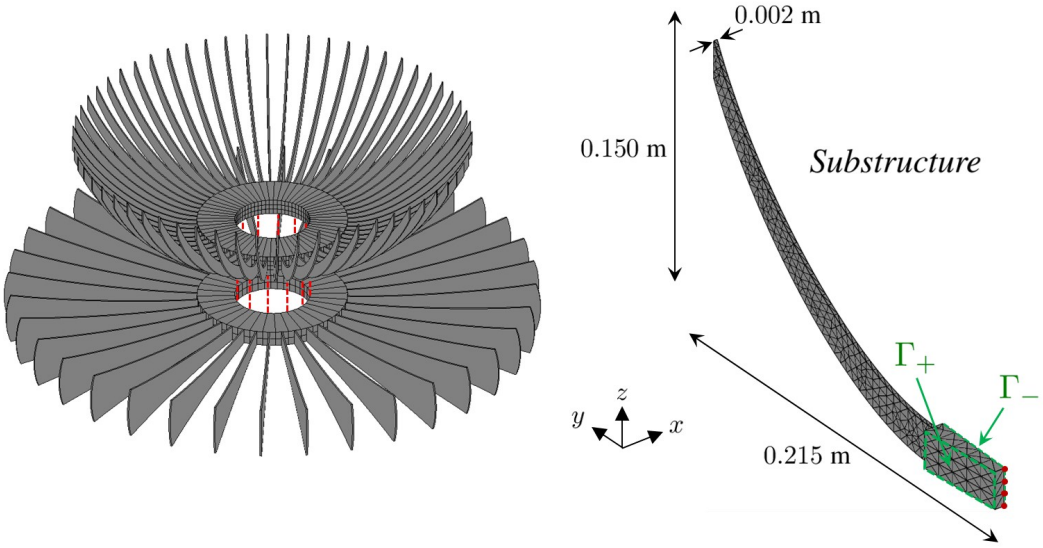

Figure 8: Assembly made up of one structure P36 and one structure P60 (left), and FE mesh of a substructure composing the structure P60 (right).

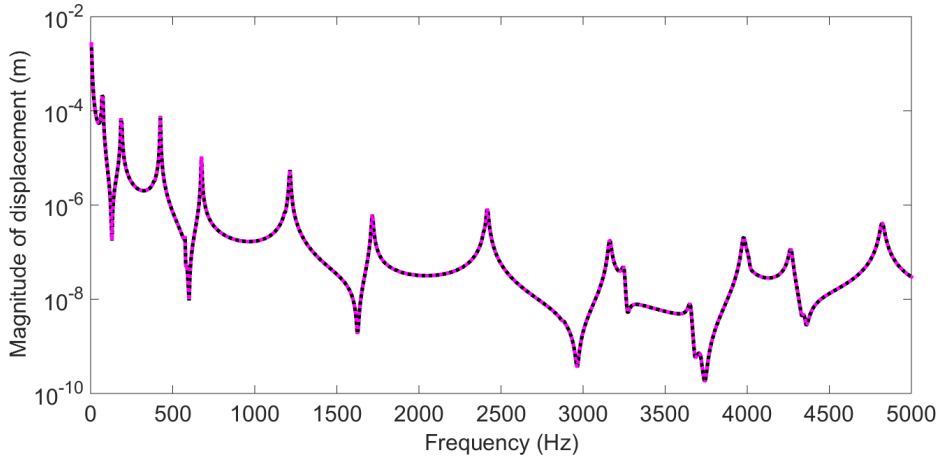

Figure 9: FRF of the assembly made up of one structure P36 and one structure P60: (black solid line) FE method; (pink dotted line) WFE approach.

with the theory of cyclic symmetry. Here, a reduction of 74% of the computational time involved in the FE method can be achieved with the WFE approach, which appears to be better compared to the single structure case (see Table 1). The computational burden of the FE method is mainly due to the computation of the DSM of the whole structural assembly. This is done by building the DSMs of the periodic structures, separately, from the condensed DSMs of the substructures, and assembling these by considering the displacement compatibility conditions at the coupling nodes.

Table 2: CPU times involved (two structures).

Approach used	CPU time	Reduction
FE	1656 s	
WFE	425 s	74%
Cyclic	477 s	71%

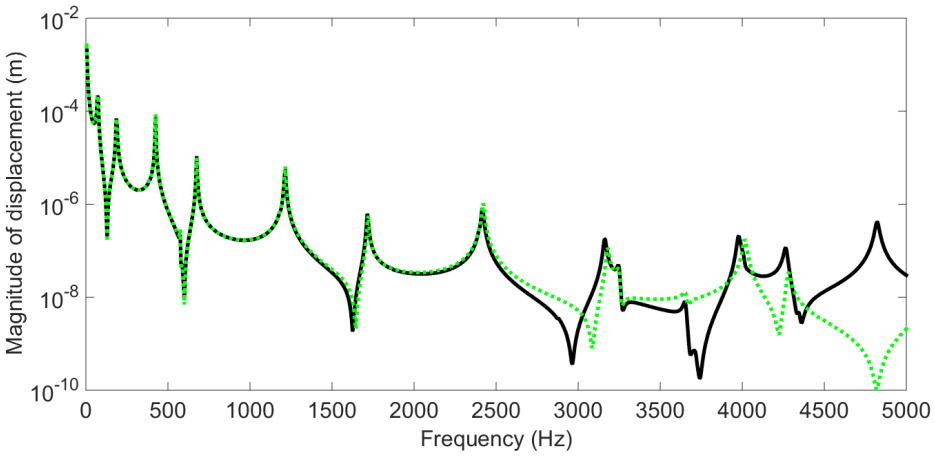

Figure 10: FRF of the assembly made up of one structure P36 and one structure P60: (black solid line) FE method; (green dotted line) theory of cyclic symmetry.

To further highlight the efficiency of the WFE approach, a second numerical example involving substructures with more DOFs is considered as shown in Figure 11. Recall that, in this case, 7482 and 4878 DOFs are used to mesh the substructures (for P36 and P60, respectively), and $n_1 = 216$ and $n_2 = 315$ DOFs are used to mesh the substructure interfaces (respectively). Also, the magnitudes of the forces acting along the circumferential direction of structure P36 are slightly perturbed to break the cyclically symmetry properties of the excitation conditions. The boundary DOFs which are considered to model the substructures are highlighted in red spots in Figure 11.

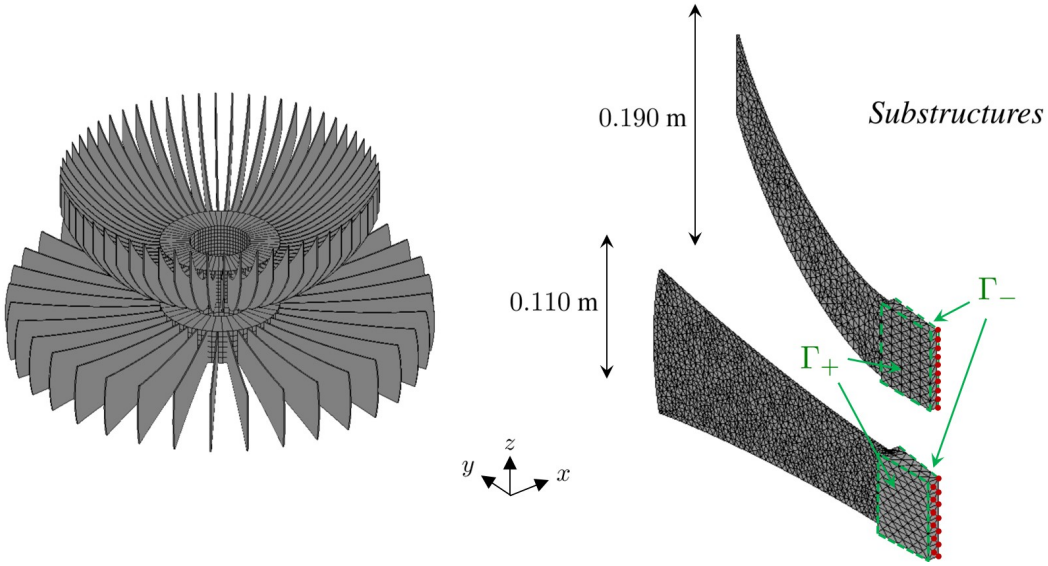

Figure 11: Assembly made up of one structure P36 and one structure P60 with more DOFs (left), and FE meshes of the substructures composing the structures P36 and P60 (right).

The FRF of the assembly involving these new structures P36 and P60 is computed with the FE method, the WFE approach and the theory of cyclic symmetry as shown in Figures 12 and 13. Again, the WFE curve perfectly matches the FE solution over the whole frequency band (see Figure 12). Here, the FRF shows several resonance peaks which are not uniformly spread on the frequency band. The dynamic behavior of the structural assembly appears to be more complex compared to the previous case, which is partly due to the change of the excitation conditions (non symmetric case), and also to the extended frequency range. Again, the accuracy

of the WFE approach is well established. In contrast, the theory of cyclic symmetry provides poor results, especially between 1500 Hz and 6000 Hz as shown in Figure 13. The drawback of the theory has been explained previously, and is due to the fact that the coupling between the harmonic modes of the periodic structures is not taken into account in the modeling of the assembly.

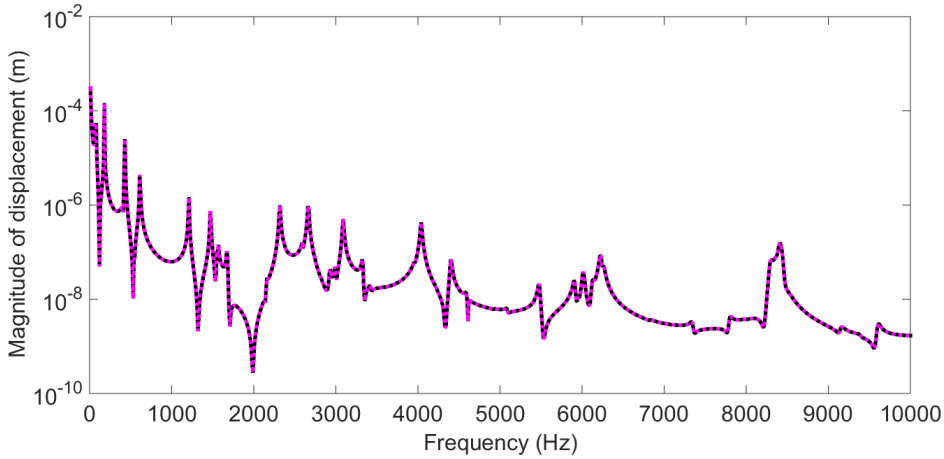

Figure 12: FRF of the assembly made up of two structures P36 and P60 with more DOFs: (black solid line) FE method; (pink dotted line) WFE approach.

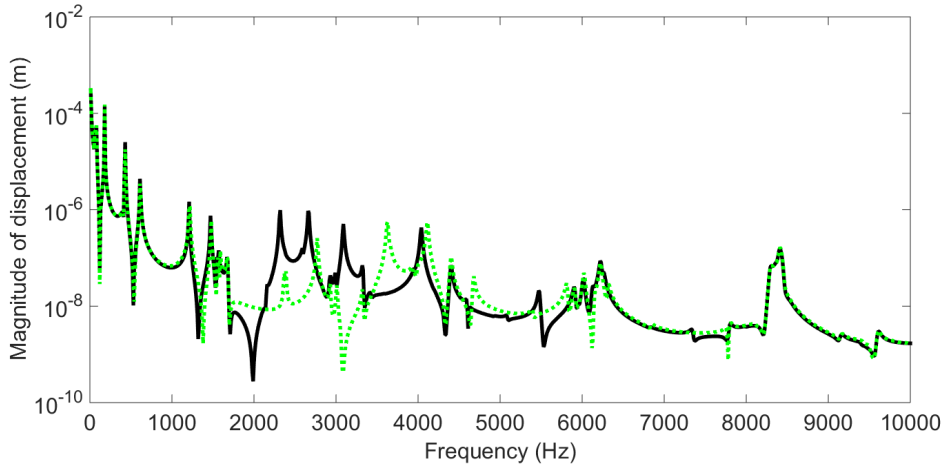

Figure 13: FRF of the assembly made up of two structures P36 and P60 with more DOFs: (black solid line) FE method; (green dotted line) theory of cyclic symmetry.

The CPU times involved in the three approaches (FE, WFE, cyclic symmetry) are displayed in Table 3. It is seen that the WFE approach shows CPU times which remain (i) of the same order as the theory of cyclic symmetry, and (ii) small compared to the FE method (reduction of 71%).

Table 3: CPU times involved (two structures with more DOFs).

Approach used	CPU time	Reduction
FE	17750 s	
WFE	5063 s	71%
Cyclic	4592 s	74%

3.3. Three periodic structures

A last test case is considered to further highlight the efficiency of the WFE approach compared to the FE method. In this case, an assembly made up of three periodic structures — i.e., two bottom structures P36 and one top structure P60 — is considered as shown in Figure 14. The upper periodic structures P36 and P60 are coupled in the same way as the previous case (see Figure 8) — i.e., using twelve nodes — while 36 nodes are used to couple the two structures P36. Note that the characteristics of the structures P36 and P60 are similar to those depicted in Figures 5 and 8.

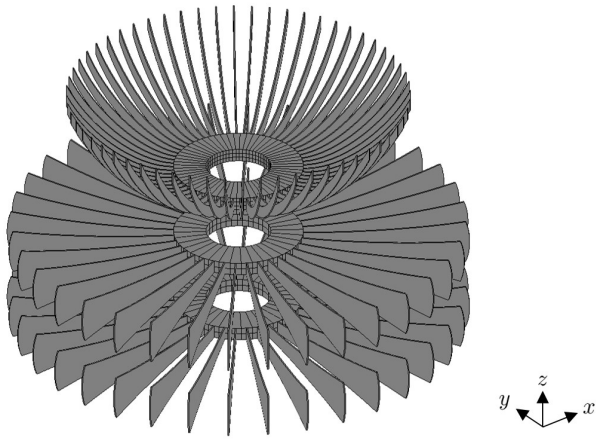

Figure 14: Assembly made up of two structures P36 and one structure P60.

The FRFs issued from the FE method and the WFE approach are shown in Figure 15. Again, the accuracy of the WFE approach can be clearly highlighted. In this case, a reduction of 78% of the computational time involved in the FE method can be achieved with the WFE approach (see Table 4), which appears to be better compared to the previous test cases. It means that the WFE approach becomes more and more efficient as the number of periodic structures considered increases. This fully gives credit to the proposed approach to address the dynamic response of assemblies made up of several periodic structures like those involved in the aeronautic industry (e.g., propellers with multi-stage disks).

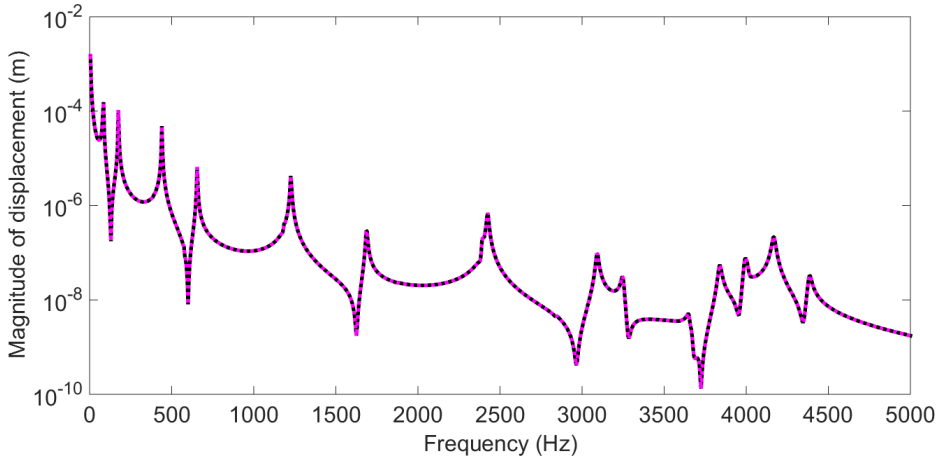

Figure 15: FRF of the assembly made up of two structures P36 and one structure P60: (black solid line) FE method; (pink dotted line) WFE approach.

Table 4: CPU times involved (three structures).

Approach used	CPU time	Reduction
FE	1960 s	
WFE	430 s	78%

4. Conclusion

A WFE approach has been proposed to model periodic structures with cyclic symmetry, and assemblies made up of these periodic structures. The key idea behind the proposed approach consists of considering the wave modes of periodic structures and using these as a means to express the matrices of dynamic flexibility modes of these structures. The modeling of assemblies made up of several periodic structures involves considering a coupling problem of small size whose resolution can be quickly achieved. Numerical experiments have been proposed which clearly highlight the efficiency of the WFE approach compared to the FE method and the theory of cyclic symmetry.

Appendix. Derivation of Eq. (36)

Let us rewrite the matrices occurring in Eq. (35) as follows:

$$\begin{bmatrix} \boldsymbol{\Phi}_{\mathrm{q}}\boldsymbol{\mu}^{N-1} & \boldsymbol{\Phi}_{\mathrm{q}}^{\star} \\ \boldsymbol{\Phi}_{\mathrm{q}} & \boldsymbol{\Phi}_{\mathrm{q}}^{\star}\boldsymbol{\mu}^{N-1} \end{bmatrix} = \begin{bmatrix} \boldsymbol{\Phi}_{\mathrm{q}}\boldsymbol{\mu}^{N-1} & \boldsymbol{\Phi}_{\mathrm{q}}^{\star}\boldsymbol{\mu}^{N} \\ \boldsymbol{\Phi}_{\mathrm{q}}\boldsymbol{\mu}^{N} & \boldsymbol{\Phi}_{\mathrm{q}}^{\star}\boldsymbol{\mu}^{N-1} \end{bmatrix} + \begin{bmatrix} \mathbf{0} & \boldsymbol{\Phi}_{\mathrm{q}}^{\star}(\mathbf{I}_n - \boldsymbol{\mu}^{N}) \\ \boldsymbol{\Phi}_{\mathrm{q}}(\mathbf{I}_n - \boldsymbol{\mu}^{N}) & \mathbf{0} \end{bmatrix}, \tag{A-1}$$

and

$$\begin{bmatrix} -\boldsymbol{\Phi}_{\mathrm{F}}\boldsymbol{\mu}^{N-1} & -\boldsymbol{\Phi}_{\mathrm{F}}^{\star} \\ \boldsymbol{\Phi}_{\mathrm{F}} & \boldsymbol{\Phi}_{\mathrm{F}}^{\star}\boldsymbol{\mu}^{N-1} \end{bmatrix} = \begin{bmatrix} -\boldsymbol{\Phi}_{\mathrm{F}}\boldsymbol{\mu}^{N-1} & -\boldsymbol{\Phi}_{\mathrm{F}}^{\star}\boldsymbol{\mu}^{N} \\ \boldsymbol{\Phi}_{\mathrm{F}}\boldsymbol{\mu}^{N} & \boldsymbol{\Phi}_{\mathrm{F}}^{\star}\boldsymbol{\mu}^{N-1} \end{bmatrix} + \begin{bmatrix} \mathbf{0} & -\boldsymbol{\Phi}_{\mathrm{F}}^{\star}(\mathbf{I}_n - \boldsymbol{\mu}^{N}) \\ \boldsymbol{\Phi}_{\mathrm{F}}(\mathbf{I}_n - \boldsymbol{\mu}^{N}) & \mathbf{0} \end{bmatrix}. \tag{A-2}$$

As a result of the eigenproblem (25) and the dynamic equilibrium equation of a non-excited substructure (Eq. (12)), one has:

$$\widehat{\mathbf{D}}^{*}\begin{bmatrix} \boldsymbol{\Phi}_{\mathrm{q}} \\ \boldsymbol{\Phi}_{\mathrm{q}}\boldsymbol{\mu} \end{bmatrix} = \begin{bmatrix} -\boldsymbol{\Phi}_{\mathrm{F}} \\ \boldsymbol{\Phi}_{\mathrm{F}}\boldsymbol{\mu} \end{bmatrix} \quad , \quad \widehat{\mathbf{D}}^{*}\begin{bmatrix} \boldsymbol{\Phi}_{\mathrm{q}}^{\star}\boldsymbol{\mu} \\ \boldsymbol{\Phi}_{\mathrm{q}}^{\star} \end{bmatrix} = \begin{bmatrix} -\boldsymbol{\Phi}_{\mathrm{F}}^{\star}\boldsymbol{\mu} \\ \boldsymbol{\Phi}_{\mathrm{F}}^{\star} \end{bmatrix}. \tag{A-3}$$

Eq. (A-3) simply means that the amplitudes for the positive-going wave modes vary as $\mathbf{I}_n \to \boldsymbol{\mu}$ between the interfaces Γ_- and Γ_+ of a substructure, while the amplitudes for the negative-going wave modes vary as $\mathbf{I}_n \to \boldsymbol{\mu}^{-1}$, i.e., $\boldsymbol{\mu} \to \mathbf{I}_n$.

Hence, Eq. (A-3) leads to:

$$\widehat{\mathbf{D}}^{*}\begin{bmatrix} \boldsymbol{\Phi}_{\mathrm{q}}\boldsymbol{\mu}^{N-1} & \boldsymbol{\Phi}_{\mathrm{q}}^{\star}\boldsymbol{\mu}^{N} \\ \boldsymbol{\Phi}_{\mathrm{q}}\boldsymbol{\mu}^{N} & \boldsymbol{\Phi}_{\mathrm{q}}^{\star}\boldsymbol{\mu}^{N-1} \end{bmatrix} = \begin{bmatrix} -\boldsymbol{\Phi}_{\mathrm{F}}\boldsymbol{\mu}^{N-1} & -\boldsymbol{\Phi}_{\mathrm{F}}^{\star}\boldsymbol{\mu}^{N} \\ \boldsymbol{\Phi}_{\mathrm{F}}\boldsymbol{\mu}^{N} & \boldsymbol{\Phi}_{\mathrm{F}}^{\star}\boldsymbol{\mu}^{N-1} \end{bmatrix}. \tag{A-4}$$

By considering Eqs. (A-1)-(A-4), Eq. (35) can be rewritten as follows:

$$\begin{aligned} \widehat{\mathbf{D}}^{*}\begin{bmatrix} \mathbf{0} & \boldsymbol{\Phi}_{\mathrm{q}}^{\star}(\mathbf{I}_n - \boldsymbol{\mu}^{N}) \\ \boldsymbol{\Phi}_{\mathrm{q}}(\mathbf{I}_n - \boldsymbol{\mu}^{N}) & \mathbf{0} \end{bmatrix}\begin{bmatrix} \mathbf{Q} \\ \mathbf{Q}^{\star} \end{bmatrix} \\ = \begin{bmatrix} \mathbf{0} & -\boldsymbol{\Phi}_{\mathrm{F}}^{\star}(\mathbf{I}_n - \boldsymbol{\mu}^{N}) \\ \boldsymbol{\Phi}_{\mathrm{F}}(\mathbf{I}_n - \boldsymbol{\mu}^{N}) & \mathbf{0} \end{bmatrix}\begin{bmatrix} \mathbf{Q} \\ \mathbf{Q}^{\star} \end{bmatrix} + \mathcal{H}\boldsymbol{\Theta}_{\Gamma_{\mathrm{B}}}\mathbf{F}_{\mathrm{B}}. \end{aligned} \tag{A-5}$$

Further simple decompositions of the matrices occurring in Eq. (A-5) lead to the expected result.

References

[1] O. C. Zienkiewicz, R. L. Taylor, The Finite Element Method (first volume), Butterworth-Heinemann, fifth edition, Oxford, 2000.

[2] E. Balmes, I. Bucher, Accounting for rotation in a multi-stage cyclo-symmetric model - a case study, Proceedings of the 24th International Conference on Noise and Vibration engineering (ISMA2010), Leuven, Belgium (2010) 1058–1064.

[3] D. Laxalde, J.-P. Lombard, F. Thouverez, Dynamics of Multistage Bladed Disks Systems, Journal of Engineering for Gas Turbines and Power 129 (4) (2007) 1058–1064.

[4] J.-M. Mencik, M. N. Ichchou, A substructuring technique for finite element wave propagation in multi-layered systems, Computer Methods in Applied Mechanics and Engineering 197 (6-8) (2008) 505–523.

[5] B. Mace, D. Duhamel, M. Brennan, L. Hinke, Finite element prediction of wave motion in structural waveguides, Journal of the Acoustical Society of America 117 (2005) 2835.

[6] L. Gry, C. Gontier, Dynamic modelling of railway track: a periodic model based on a generalized beam formulation, Journal of Sound and Vibration 199 (4) (1997) 531–558.

[7] J. Signorelli, A. von Flotow, Wave propagation, power flow, and resonance in a truss beam, Journal of Sound and Vibration 126 (1) (1988) 127–144.

[8] Y. Waki, B. Mace, M. Brennan, Free and forced vibrations of a tyre using a wave/finite element approach, Journal of Sound and Vibration 323 (3-5) (2009) 737–756.

[9] E. Nobrega, F. Gautier, A. Pelat, J. D. Santos, Vibration band gaps for elastic metamaterial rods using wave finite element method, Mechanical Systems and Signal Processing 79 (2016) 192–202.

[10] J.-M. Mencik, M. N. Ichchou, Wave finite elements in guided elastodynamics with internal fluid, International Journal of Solids and Structures 44 (2007) 2148–2167.

[11] E. Manconi, B. Mace, R. Gaziera, Wave finite element analysis of fluid-filled pipes, Proceedings of NOVEM 2009 “Noise and Vibration: Emerging Methods”, Oxford, UK.

[12] Q. Serra, M. N. Ichchou, J. F. Deü, Wave properties in poroelastic media using a Wave Finite Element Method, Journal of Sound and Vibration 335 (2015) 125–146.

[13] P. Silva, J.-M. Mencik, J. Arruda, Wave finite element-based superelements for forced response analysis of coupled systems via dynamic substructuring, International Journal for Numerical Methods in Engineering 107 (6) (2016) 453–476.

[14] J.-M. Mencik, On the low- and mid-frequency forced response of elastic systems using wave finite elements with one-dimensional propagation, Computers and Structures 88 (11-12) (2010) 674–689.

[15] D. Duhamel, B. Mace, M. J. Brennan, Finite element analysis of the vibrations of waveguides and periodic structures, Journal of Sound and Vibration 294 (1-2) (2006) 205–220.

[16] Y. Waki, B. Mace, M. Brennan, Numerical issues concerning the wave and finite element method for free and forced vibrations of waveguides, Journal of Sound and Vibration 327 (1-2) (2009) 92–108.

[17] D. Mead, The forced vibration of one-dimensional multi-coupled periodic structures: An application to finite element analysis, Journal of Sound and Vibration 319 (2009) 282–304.

[18] B. Mace, E. Manconi, Modelling wave propagation in two-dimensional structures using finite element analysis, Journal of Sound and Vibration 318 (4-5) (2008) 884–902.

[19] J.-M. Mencik, D. Duhamel, A wave-based model reduction technique for the description of the dynamic behavior of periodic structures involving arbitrary-shaped substructures and large-sized finite element models, Finite Elements in Analysis and Design 101 (2015) 1–14.

[20] R. R. Craig, M. C. C. Bampton, Coupling of substructures for dynamic analyses, AIAA Journal 6 (7) (1968) 1313–1319.

[21] J.-M. Mencik, M. N. Ichchou, Multi-mode propagation and diffusion in structures through finite elements, European Journal of Mechanics - A/Solids 24 (5) (2005) 877–898.

[22] W. X. Zhong, F. W. Williams, On the direct solution of wave propagation for repetitive structures, Journal of Sound and Vibration 181 (3) (1995) 485–501.

[23] J.-M. Mencik, New advances in the forced response computation of periodic structures using the wave finite element (WFE) method, Computational Mechanics 54 (3) (2014) 789–801.

[24] D. Klerk, D. J. Rixen, J. de Jong, The frequency based substructuring (fbs) method reformulated according to the dual domain decomposition method, in: Proceedings of IMAC-XXIV: Conference & Exposition on Structural Dynamics, no. 136, St. Louis, 2006, p. 14.

[25] M. Legrand, C. Pierre, P. Cartraud, J.-P. Lombard, Two-dimensional modeling of an aircraft engine structural bladed disk-casing modal interaction, Journal of Sound and Vibration 319 (1-2) (2009) 366–391.